Fabric- and fluid-constrained $^{40}Ar/^{39}Ar$ geochronology of the northeastern Carajás Province, Amazonian Craton: separating hydrothermalism from Rhyacian and Orosirian reworking of Archean crust

Felipe Mattos Tavares[a], Rudolph Allard Johannes Trouw[b], Paulo Marcos Vasconcelos[c]

[a] Geological Survey of Brazil (SGB/CPRM), Rio de Janeiro, RJ, Brazil
[b] Instituto de Geociências, Universidade Federal do Rio de Janeiro, Rio de Janeiro, RJ, Brazil
[c] School of the Environment, The University of Queensland, Brisbane, QLD, Australia

Corresponding author: Felipe Mattos Tavares — fmatav@gmail.com

The complete $^{40}Ar/^{39}Ar$ analytical dataset is openly available in Mendeley Data at https://doi.org/10.17632/cgx6zx9m3n.1

Fabric- and fluid-constrained $^{40}Ar/^{39}Ar$ geochronology of the northeastern Carajás Province, Amazonian Craton: separating hydrothermalism from Rhyacian and Orosirian reworking of Archean crust

Felipe Mattos Tavares[a,b]*, Rudolph Allard Johannes Trouw[b], Paulo Marcos Vasconcelos[c]

[a] Serviço Geológico do Brasil (SGB/CPRM), Av. Pasteur 404, Urca, Rio de Janeiro, RJ, 22290-255, Brazil

[b] Programa de Pós-Graduação em Geologia, Universidade Federal do Rio de Janeiro, Av. Athos da Silveira Ramos 274, Cidade Universitária, Ilha do Fundão, Rio de Janeiro, RJ 21941-916, Brazil.

[c] School of the Environment, The University of Queensland, Brisbane, QLD 4072, Australia

* Corresponding author. E-mail address: fmatav@gmail.com (F.M. Tavares).

Abstract

The Carajás Province, southeastern Amazonian Craton, is a polycyclic Archean block in which the ages of rocks, hydrothermal minerals and tectonic fabrics need not coincide. We integrate multiscale structural analysis with fabric-constrained $^{40}Ar/^{39}Ar$ geochronology of amphibole, biotite and white mica selected from mapped fabrics or well-defined hydrothermal assemblages. Although the province preserves a dominantly Archean rock record, minerals defining its main foliation yield Paleoproterozoic recrystallization ages. Hornblende and biotite tied to that fabric record a Rhyacian Transamazonian event at ca. 2.08–2.05 Ga. A distinct Early Orosirian Sereno event at ca. 2.01–1.96 Ga is recorded by anthophyllite–tremolite and biotite, whereas white mica near Serra Pelada yields ca. 1.93 Ga minimum constraints partially reset toward a ca. 1.88 Ga Uatumã overprint. Hydrothermal amphiboles preserve a polyphase Neoarchean record. Substantial Serra Verde fractions overlap the Re–Os molybdenite age, and the principal surviving amphibole reservoirs yield

2516 ± 14 and 2517 ± 12 Ma. In the stretched FT-009C hydrothermal pocket, exploratory arrays at 2199 ± 25 and 2087 ± 31 Ma record selective fluid-assisted re-equilibration and deformation-related recrystallization. Cl/K systematics identify fluid-hosted excess ^{40}Ar and separate inherited reservoirs from geological age components. The exposed architecture is therefore an Archean crustal block pervasively reworked during distinct Paleoproterozoic events, with domain-scale recrystallization controlling the survival of older argon reservoirs.

Highlights

• Carajás' main regional foliation records Rhyacian recrystallization.

• Fabric-hosted biotite and hornblende date collision at 2.08–2.05 Ga.

• Early Orosirian Sereno reworking occurred at 2.01–1.96 Ga.

• Cl/K resolves a polyphase ca. 2.61–2.52 Ga hydrothermal amphibole record.

• Hydrothermal amphiboles record ca. 2.20 Ga fluid and ca. 2.09 Ga strain reworking.

Keywords: $^{40}Ar/^{39}Ar$ geochronology; Carajás Province; Amazonian Craton; Transamazonian orogeny; fabric recrystallization; Paleoproterozoic reworking

1. Introduction

Archean cratons commonly preserve old crustal nuclei whose present architecture records more than the age of their protoliths (Holdsworth et al., 1997). Along cratonic margins, older assemblages may be shortened, hydrated, cooled, reactivated and partially overprinted during younger orogenic cycles without producing abundant new zircon or resetting high-temperature isotopic systems. The central problem is then not to date the host rocks but to determine whether the fabrics they preserve are themselves Archean or record later tectono-thermal events. This matters most in mineralized cratonic provinces, where magmatic, metamorphic, structural and hydrothermal ages overlap spatially but correspond to different processes.

The Carajás Province, in the southeastern Amazonian Craton, is an ideal setting for such a study: a block whose tectonic evolution, deformation, metamorphism and associated hydrothermal and mineralizing processes are superimposed and cannot be separated by rock ages alone. Its rock-generation record is dominantly Archean, including Mesoarchean basement, Neoarchean volcano-sedimentary sequences of the Itacaiúnas Supergroup, mafic–ultramafic complexes, A-type granitoids and major iron oxide–copper–gold (IOCG) systems (Machado et al., 1991; Dall'Agnol et al., 2005; Monteiro et al., 2008; Xavier et al., 2012; Moreto et al., 2015a, b). A younger anorogenic event at ca. 1.88 Ga is represented by Uatumã-related A-type magmatism and hydrothermal alteration (Dall'Agnol et al., 2005; Grainger et al., 2008; Ferron et al., 2010; Pollard et al., 2019). Between these two age domains lies the central problem addressed here: the age of the regional fabrics and metamorphic overprints preserved in Archean host rocks.

Resolving this history requires structural analysis integrated across scales. Macro-scale mapping defines the province-scale fabrics and their overprinting relationships, meso-scale observations characterize foliations, crenulations and shear fabrics, and microtectonics establishes which minerals grew or recrystallized within each fabric. Only when a dated mineral can be tied to a fabric at all three scales can its age be assigned to a deformation or metamorphic event instead of host-rock formation.

The $^{40}Ar/^{39}Ar$ method is well suited to this problem when applied to minerals whose textural significance is well understood. Step-heating analysis of amphiboles, biotite and white micas can record recrystallization and cooling through mineral-specific argon-retention windows, while also exposing excess Ar, disturbed low-temperature steps, partial resetting and mixed gas reservoirs (Dodson, 1973; Berger, 1975; Harrison, 1981; McDougall and Harrison, 1999). It is now widely recognized that, in polymetamorphic rocks, the argon record of micas and amphiboles is governed less by simple volume diffusion than by fluid-assisted recrystallization. Without fluids or retrograde reactions these minerals can retain argon to unexpectedly high temperatures, but recrystallization resets them efficiently even at low grade (Villa, 2016; Montemagni and Villa, 2025). Recent applications in Archean and Proterozoic terranes exploit this behaviour, linking mineral ages to deformation, fluid flow and partial resetting and not host-rock crystallization alone (Caswell et al., 2021; Scheiber et al., 2023; Chagondah et al., 2024; Billström et al., 2025; Montemagni and Villa, 2025). Two consequences guide this study. A $^{40}Ar/^{39}Ar$ age dates the last recrystallization of the analyzed volume rather than the birth of the fabric hosting it; and a mineral that grew or recrystallized within a mapped fabric constrains that fabric-forming event, whereas one belonging to a vein or alteration assemblage instead dates fluid circulation or mineralization.

Available K–Ar and $^{40}Ar/^{39}Ar$ data had already suggested that the thermal evolution of Carajás was more complex than indicated by U–Pb, Pb–Pb and Re–Os datasets alone (Gomes et al., 1975; Renne et al., 1988). Most of those ages lacked direct structural control, and many Rhyacian–Orosirian dates came from accessory phases in mineralized or texturally complex settings, so Paleoproterozoic ages were commonly grouped within a broad "Transamazonian" interval (2.20-1.95 Ga) without separating tectonic recrystallization, fabric formation, hydrothermal disturbance and later resetting. Comparable $^{40}Ar/^{39}Ar$ studies in the Guiana Shield show that Archean rocks can be completely reset during Transamazonian tectono-metamorphism (Rosa-Costa et al., 2009). Carajás requires a similar but more explicitly fabric-constrained treatment.

Earlier tectonic models commonly related the main structural fabrics of northern Carajás to long-lived Archean strike-slip systems, later reactivated under transpressional or transtensional regimes (Araújo et al., 1988; Costa et al., 1995; Pinheiro and Holdsworth, 1997, 2000; Holdsworth and Pinheiro, 2000). Regional mapping and structural analysis led Tavares et al. (2018) to reinterpret the northeastern Carajás Province as a polycyclic margin affected by successive extensional and compressional events: a Rhyacian Transamazonian event related to Carajás–Bacajá collision, crustal thickening, province-scale foliation development and a northward-increasing metamorphic gradient; a younger Early Orosirian overprint, the Sereno Event, reorganizing that fabric under lower-grade, intraplate conditions; and post-Sereno extension and hydrothermal reactivation linked to the ca. 1.88 Ga Uatumã system.

Here we present a $^{40}Ar/^{39}Ar$ dataset from structurally controlled samples along a north–south transect across the northeastern Carajás Province, spanning Archean basement, Neoarchean supracrustal and intrusive rocks, Paleoproterozoic cover units and major structurally controlled domains (Figs. 1, 2). We dated amphiboles (hornblende, actinolite, anthophyllite, tremolite), biotite and white mica (muscovite, sericite) selected from mapped fabrics or from well-defined hydrothermal assemblages, and we use the chlorine, calcium and potassium systematics inherent to the $^{40}Ar/^{39}Ar$ measurements to distinguish mineral and gas reservoirs. We test whether the present-day foliation architecture of Carajás is fundamentally Neoarchean or Paleoproterozoic, separate Transamazonian and Sereno thermal histories, and distinguish both from the younger Uatumã-related hydrothermal overprint.

Beyond its regional implications, the resulting time-resolved thermal archive shows how structurally controlled $^{40}Ar/^{39}Ar$ data can resolve temporally distinct episodes of deformation, cooling and fluid circulation that would otherwise remain grouped within broad

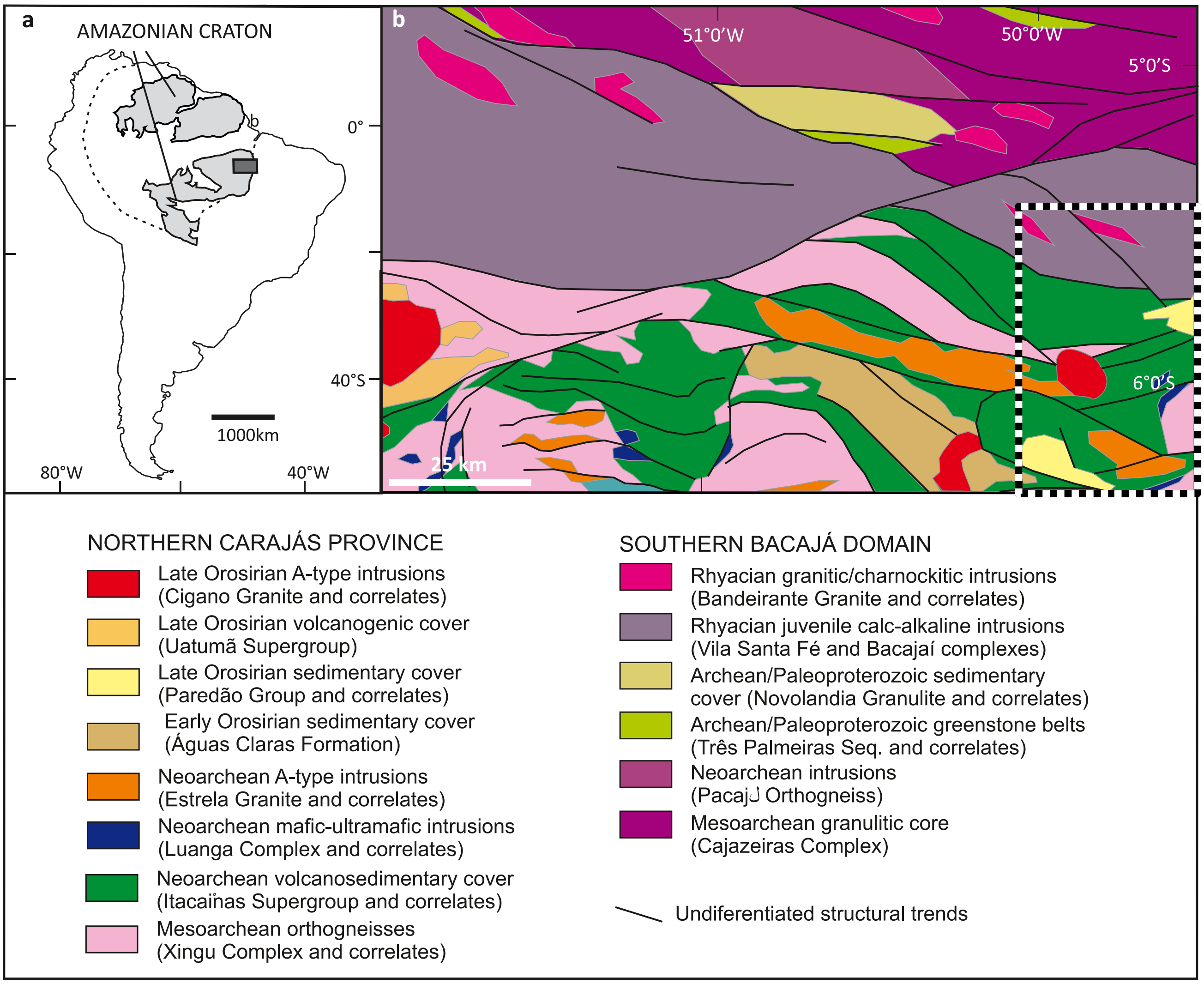

Figure 1. Regional geological map of the northeastern Carajás Province and the adjacent southern Bacajá Domain, southeastern Amazonian Craton, showing the main lithostratigraphic units and structural trends. The dashed box outlines the study area (Fig. 2); inset (a) locates the Amazonian Craton within South America. Modified from Costa et al. (2016) and Tavares et al. (2018).

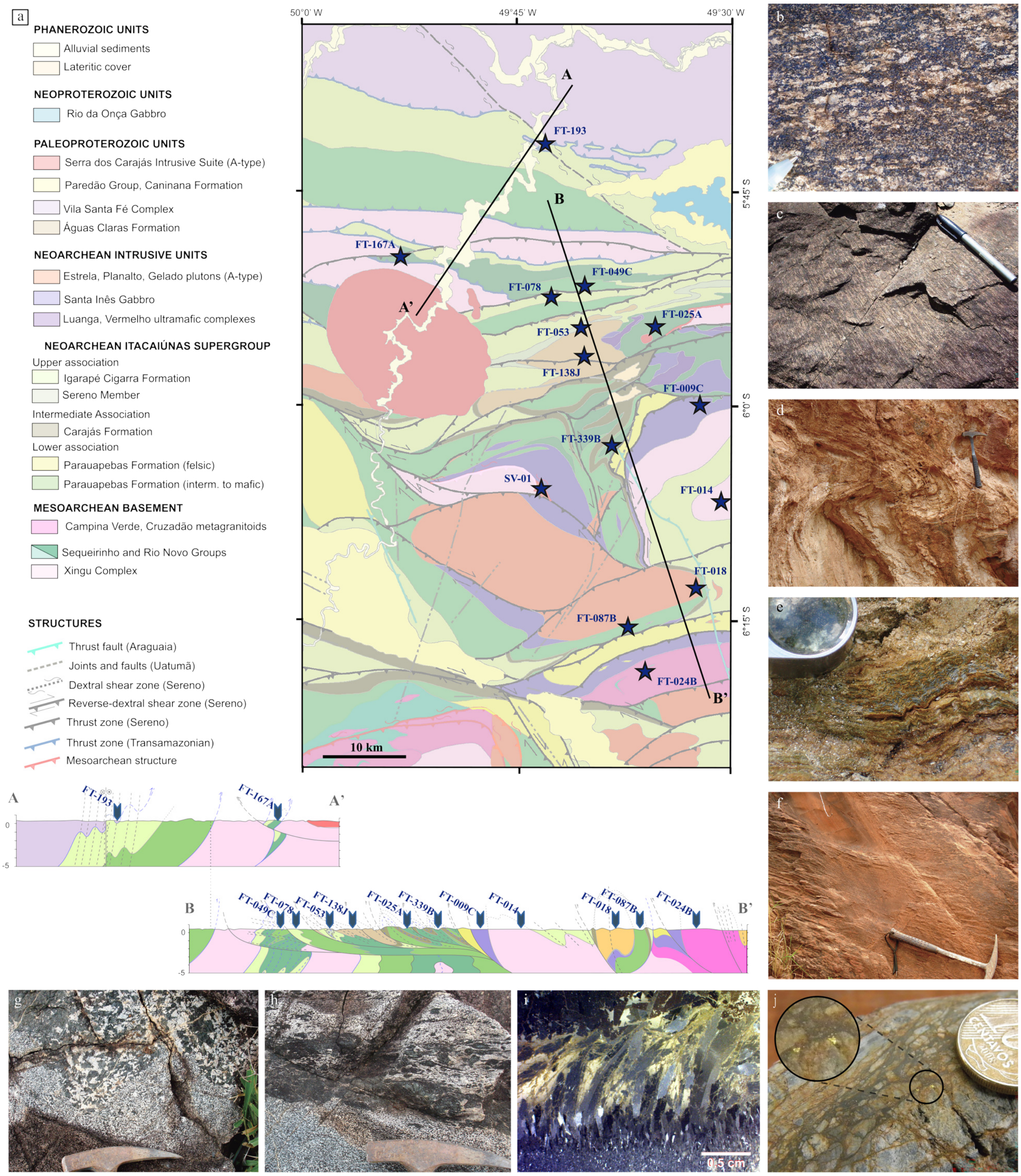

Figure 2. Regional structures, dated localities and field relations. (a) Geological map and structural cross-sections A–A′ and B–B′, with locations of the $^{40}Ar/^{39}Ar$ samples. (b) FT-193 mafic granulite, whose foliation is marked by oriented intergrowths of plagioclase, amphibole and pyroxene. (c) Parauapebas Formation amphibolite at FT-166, tens of metres from FT-167, showing a pronounced down-dip Transamazonian stretching lineation. (d) Metasedimentary and metamafic rocks of the upper Itacaiúnas Supergroup near FT-078, where the Transamazonian foliation is folded by Sereno deformation into low-angle, recumbent folds. (e) Upper Itacaiúnas metasedimentary rocks at Serra Pelada region, with Transamazonian foliation crenulated by Sereno deformation. (f) Interbedded metasiltstone and fine metarenite of the Águas Claras Formation at FT-138, adjacent to the Serra Pelada artisanal mine, where low-angle Sereno cleavage truncates steep sedimentary bedding. (g, h) Amphibole–plagioclase hydrothermal pockets in Luanga Complex metagabbro at FT-009, preserving coarse textures in plan view (g) and tectonic stretching in a section parallel to the lineation (h). (i) Syntaxial amphibole vein near Serra Verde, sheared by a Transamazonian ductile structure; strain is concentrated around and penetrates the amphibole megacrysts poorly. (j) Drill core from the Serra Pelada Au–Pt–Pd mineralization, hosted by fine metarenite of the Águas Claras Formation. An oriented fracture-breccia system is interpreted as a carbonaceous-fluid-assisted tectonic breccia within a linear structure; the enlarged view shows two submillimetre particles of native Au at the contact between the carbonaceous matrix and the structure wall. Map modified from Tavares and Silva (2015) and Tavares (2014); cross-sections modified from Tavares et al. (2018).

regional age domains. The approach applies to other polycyclic Precambrian terranes in which inherited lithologies preserve younger fabrics and multiple generations of isotopic disturbance.

2. Tectonostratigraphic setting

The Carajás Province forms the southeastern part of the Amazonian Craton and is classically distinguished from the Paleoproterozoic Transamazonas (Transamazonian) or Maroni-Itacaiúnas Province to the north (Cordani et al., 1984; Teixeira et al., 1989; Santos, 2003; Vasquez and Rosa-Costa, 2008). In this regional framework Carajás represents the main Archean nucleus of the eastern craton, whereas the Bacajá and related domains expose Paleoproterozoic crust involved in the Transamazonian evolution. The study area lies along the northeastern margin of the Carajás Province, close to the Carajás–Bacajá boundary (Fig. 1) and west of the Neoproterozoic–Cambrian Araguaia Belt, related to the Brasiliano Cycle (Hasui et al., 1977; Paixão et al., 2008).

The basement of the Carajás Domain comprises the oldest exposed crust of the southern Amazonian Craton. In the northern part of the province, it includes high-grade TTG orthogneisses and orthogranulites, granitoid–gneiss associations and greenstone fragments commonly grouped within the Xingu Complex and related units. U–Pb zircon ages indicate crystallization of older TTG components between ca. 3.08 and 2.95 Ga, followed by greenstone-related magmatism near 2.97 Ga and emplacement of crustal-melt granitoids between ca. 2.87 and 2.83 Ga (Machado et al., 1991; Pidgeon and Macambira, 2000; Feio et al., 2013; Delinardo, 2014; Moreto et al., 2015a, b; Marangoanha et al., 2019). This Mesoarchean evolution was accompanied by ductile deformation and medium- to high-grade metamorphism, producing an anisotropic crustal framework dominated by E–W to ENE–WSW fabrics (Costa et al., 2016; Tavares et al., 2018).

The Neoarchean cover of the Carajás Domain is represented mainly by the Itacaiúnas Supergroup, a volcano-sedimentary succession that includes the Grão Pará Group and associated units (Fig. 2). The lower volcanogenic association comprises mafic to felsic volcanic rocks of the Parauapebas Formation and the banded iron formations of the Carajás Formation, with volcanic activity constrained at ca. 2.76–2.73 Ga (Gibbs et al., 1986; Wirth et al., 1986; Trendall et al., 1998). Upper clastic, chemical and volcanogenic associations are grouped in the Serra da Bocaina and related units (Costa et al., 2016), although the internal stratigraphy is locally complicated by tectonic transposition, metamorphic contrasts and hydrothermal alteration. Coeval intrusive activity was bimodal, including layered mafic–ultramafic complexes such as Luanga, dated at ca. 2.76 Ga, and A-type granitoids such as the Estrela and Igarapé Gelado metagranites, emplaced between ca. 2.76 and 2.71 Ga (Machado et al., 1991; Barros et al., 2001; Barbosa, 2004; Dall'Agnol et al., 2005).

This Neoarchean stage also established much of the mineral-system architecture of Carajás. Extensive Na to Na-Ca alteration, magnetite-rich hydrothermal assemblages and IOCG systems overprint both basement and supracrustal units, with major ore-forming and alteration ages between ca. 2.71 and 2.54 Ga (Monteiro et al., 2008; Xavier et al., 2012; Moreto et al., 2015a, b; Melo et al., 2017; Trunfull et al., 2020; Schutesky and Oliveira, 2020).

The Paleoproterozoic evolution of Carajás is the central issue for this study. Early geochronological syntheses recognized a broad Paleoproterozoic thermal overprint between ca. 2.10 and 1.95 Ga in the eastern Amazonian Craton, generally discussed within a wide Transamazonian framework (Gomes et al., 1975; Cordani et al., 1984; Teixeira et al., 1989). More recent studies show larger complexity. First, an older, ca. 2.2 Ga thermal–hydrothermal signal is preserved in southern Carajás, defined by a 2193 ± 4 Ma $^{40}Ar/^{39}Ar$ biotite age at

Corta Goela (Pollard et al., 2019), a 2199 ± 13 Ma amphibole age from ore-related alteration at Sossego (Marschik et al., 2003), and a 2162.9 ± 28.1 Ma U–Pb age from hydrothermal titanite at Antas North (Hühn et al., 2025). Second, tectonostratigraphic relations separate two tectono-thermal events with distinct kinematics, metamorphic conditions and regional significance (Tavares et al., 2018): a Rhyacian Transamazonian orogeny at ca. 2.10 Ga, related to convergence and collision between the Carajás Domain and Paleoproterozoic terranes to the north, especially the Bacajá Domain; and an Early Orosirian intracontinental reworking phase, the Sereno Event, at ca. 2.00 Ga.

During the Transamazonian event, the Vila Santa Fé Complex and related Paleoproterozoic units were thrust southward over the Archean margin of Carajás. This deformation generated a province-scale ENE–WSW to WNW–ESE foliation, with dominant tectonic transport toward the S to SW and a metamorphic gradient that increases northward, from greenschist facies in the southern Carajás Domain to amphibolite- and granulite-facies assemblages near the Carajás–Bacajá boundary (Tavares and Silva, 2015; Tavares et al., 2018). The fabric affects Neoarchean supracrustal rocks, Mesoarchean basement granitoids and younger Siderian to Rhyacian assemblages of the Bacajá Domain to the north. Syn- to late-orogenic relaxation is recorded by the Águas Claras Formation, deposited unconformably over Archean assemblages (Nogueira et al., 1995; Araújo et al., 2020) and interpreted by Tavares et al. (2018) as late- to post-orogenic basin development following crustal thickening. A pronounced down-dip Transamazonian stretching lineation is exposed in Parauapebas Formation amphibolite at FT-166, tens of metres from the dated FT-167 locality (Fig. 2c). Near Serra Verde, a syntaxial amphibole vein is sheared by a Transamazonian ductile structure, with strain concentrated around the megacrysts and penetrating them poorly (Fig. 2i).

The Sereno Event overprints this Transamazonian architecture under lower-temperature conditions. It is expressed by renewed folding, crenulation cleavage, local shear zones, tectonic slicing and reactivation of older anisotropies, commonly with top-to-NNW or NW transport (Tavares et al., 2018). In the lower-grade Águas Claras cover it may generate new slaty cleavage; in rocks that already preserve a Transamazonian schistosity it forms crenulations, localized high-strain zones and partial recrystallization of mica- and amphibole-bearing assemblages. Near FT-078, Transamazonian foliation in upper Itacaiúnas metasedimentary and metamafic rocks is folded into low-angle axial-plane folds (Fig. 2d). At Serra Pelada, the same foliation is crenulated by Sereno structures (Fig. 2e). In the Águas Claras Formation at FT-138, a low-angle Sereno cleavage truncates steep bedding in interbedded metasiltstone and fine metarenite adjacent to the artisanal mine (Fig. 2f).

Carajás was broadly affected by late Orosirian extension and widespread anorogenic magmatism related to the Uatumã event, with A-type granites and volcanic rocks emplaced at ca. 1.88 Ga across the province and accompanied by granite-related hydrothermal systems, including local Au–PGE and Cu–Au mineralization (Dall'Agnol et al., 2005; Grainger et al., 2008; Ferron et al., 2010; Xavier et al., 2012; Pollard et al., 2019). Drill core from the Serra Pelada Au–Pt–Pd system shows an oriented breccia in fine Águas Claras metarenite, interpreted as a carbonaceous-fluid-assisted tectonic breccia, with native Au at the carbonaceous matrix–wall contact (Fig. 2j).

Younger overprints are more restricted. Neoproterozoic extension related to the opening of the Araguaia basin and subsequent Brasiliano inversion produced distal brittle to brittle–ductile reactivation within Carajás (Hasui et al., 1977; Tavares et al., 2018; Cruz and Gorayeb, 2020). Later mafic dyke and sill swarms, including Jurassic intrusions associated with Central Atlantic rifting, locally introduced minor thermal disturbance (Cordani, 1981; Macambira et al., 2016; Giovanardi et al., 2019; Teixeira et al., 2019).

3. Materials and methods

3.1 Sampling strategy and structural control

The sampling strategy was designed to test the age of the main tectonic fabrics preserved in the northeastern Carajás Province and to distinguish them from hydrothermal amphibole systems unrelated to penetrative deformation. Samples were collected along a north–south transect extending from the Carajás–Bacajá boundary into the southern Archean basement. The transect crosses Paleoproterozoic allochthonous units, Neoarchean supracrustal sequences, Paleoproterozoic cover rocks, major shear-zone domains and Mesoarchean granitoids. This geometry was chosen to sample minerals from different structural levels and metamorphic conditions within the same regional tectonostratigraphic framework (Fig. 2a). Mineral selection was guided by field relations, thin-section petrography and the textural position of the dated phase. Hornblende, actinolite, anthophyllite, biotite and white mica were selected where they define, recrystallize within, or are clearly overprinted by mapped fabrics, including the main regional foliation, crenulation cleavage, localized shear fabrics and mica-rich low-grade cleavages. In these samples the objective was to date recrystallization or cooling of minerals linked to tectonic fabrics and not the crystallization age of the host rocks. A second group of samples was included as hydrothermal references, in which amphibole belongs to alteration assemblages or veins associated with Cu mineralization and is not part of a penetrative tectonic fabric. Table 1 summarizes the samples retained in the main dataset, their tectonostratigraphic position, dated minerals, host-rock ages and interpretive role.

Tables

Table 1. Samples, host-rock ages, dated minerals and sampling rationale. Host-rock ages are from the literature and regional correlation as cited in the text.

Sample	Unit / locality	Lithology	Host-rock age	Dated mineral	Textural position	Rationale
FT-193	Vila Santa Fé Complex / Rio Preto granulite	Mafic granulite	~2.6 Ga (protolith); HG metam. 2.07 Ga	Hornblende	Coarse high-grade schistosity	High-grade northern amphibole near the Carajás–Bacajá boundary
FT-049C	Parauapebas Fm.	Amphibolite	2.76–2.73 Ga	Hornblende	Main penetrative foliation	Age of foliation-forming amphibole in a Neoarchean supracrustal unit
FT-167A	Rio Novo Group	Anthophyllite–tremolite schist	~2.97 Ga	Anthophyllite–tremolite	Boudinaged amphibole near shear zone	Age of recrystallized amphibole in localized deformation
FT-078	Igarapé Cigarra succession	Sillimanite–muscovite–quartz schist	< 2.76, > 2.73 Ga	Muscovite	Mica fabric + crenulation	Mica recrystallization and later sericitization
FT-138J	Águas Claras Fm. (Serra Pelada mine)	White-mica–quartz phyllite	Deposition < 2.10, > 2.00 Ga	White mica	Slaty cleavage + coaxial crenulation	Low-grade mica fabric and younger disturbed components
FT-009C	Luanga Complex	Metagabbro with hydrothermal pocket	2763 ± 2 Ma	Hornblende–actinolite	Relict coarse amphibole–plagioclase infill, subsequently stretched	Polyphase hydrothermal record and strain-related re-equilibration
SV-01	Serra Verde artisanal mine	Cu-bearing syntaxial vein	Hydrothermal molybdenite at 2609 ± 13 Ma (Marschik et al., 2005)	Amphibole	Undeformed quartz–amphibole–chalcopyrite vein; local molybdenite	Polyphase Neoarchean hydrothermal reference
FT-087B	Parauapebas Fm.	Greenschist–amphibolite	2.76–2.73 Ga	Amphibole, biotite	Main foliation + altered domains	Inherited hydrothermal amphibole vs. Rhyacian biotite closure
FT-024B	Cruzadão Metagranite	Biotite orthogneiss	2874 ± 15 Ma	Biotite	Reworked foliation in Mesoarchean granitoid	Biotite ages from reworked Archean basement fabric

3.2 Sample preparation and analytical procedure

Crushed material was cleaned successively in an ultrasonic bath with distilled water and ethanol, and then dried. From each cleaned split, 20 to 50 grains, generally 0.5 to 2 mm in size, were hand-picked under a binocular microscope. Selection favored optically clean grains belonging to the target fabric or hydrothermal assemblage.

Aliquots of five to ten grains from each sample were loaded into aluminum irradiation discs together with Fish Canyon sanidine flux monitors, using an age of 28.201 Ma (Kuiper et al., 2008). The discs were sealed in quartz vials and irradiated for 14 h at the B-1 CLICIT facility of the Radiation Center, Oregon State University, USA. After an appropriate decay period, two to four grains from each sample were analyzed by laser incremental $^{40}Ar/^{39}Ar$ step heating at the University of Queensland, following the general analytical procedures described by Vasconcelos et al. (2002). Gas released during each heating step was purified in the extraction line before isotopic measurement. Blank corrections and neutron-induced interference corrections for K- and Ca-derived argon isotopes were applied to each step, and the neutron-flux parameter J was calculated from interspersed Fish Canyon sanidine monitors. Ages were calculated using the decay constants of Min et al. (2000) and are reported with 2σ uncertainties that include the uncertainty in J; where $^{40}Ar/^{39}Ar$ ages are compared directly with U–Pb data, uncertainties additionally propagate the decay-constant and monitor-age contributions. The hydrothermal reference sample Serra Verde-01 (SV-01) was analyzed in a separate, earlier irradiation and analytical session using the same Fish Canyon age and atmospheric $^{40}Ar/^{36}Ar$; its ages are therefore directly comparable with the main dataset. Complete step-heating data, analytical parameters and age calculations are provided in the supplementary tables.

3.3 Chemical discriminators and data-reduction criteria

Because several samples contain more than one argon reservoir, we combine the age spectra with the chemical information intrinsic to the $^{40}Ar/^{39}Ar$ measurement. The Ca/K ratio (from Ca-derived ^{37}Ar over K-derived ^{39}Ar) and the Cl/K ratio (from Cl-derived ^{38}Ar over K-derived ^{39}Ar) are used, following the approach reviewed by Montemagni and Villa (2025), to discriminate mineral reservoirs, to identify alteration- and fluid-related domains, and to test whether excess ^{40}Ar is associated with Cl-bearing components. This chemical screening is applied alongside the shape of the age spectrum.

A plateau age is accepted when at least three contiguous steps comprise 50% or more of the released ^{39}Ar, are statistically coherent at the 95% confidence level and show no major internal inconsistency in K/Ca (Fleck et al., 1977). Where spectra contain coherent segments that do not fully satisfy formal plateau criteria, pseudo-plateau ages are reported only when the segment is reproducible, analytically coherent and compatible with the petrographic context. For amphiboles with saddle-shaped spectra, anomalously old apparent ages or evidence of non-atmospheric trapped argon, inverse isochron ages are preferred over apparent plateau ages; the initial $^{40}Ar/^{36}Ar$ ratio is then used to evaluate excess-Ar components, and disturbed low-temperature or analytically unstable high-temperature steps are excluded from the preferred fit. For biotite and white mica, plateau or coherent pseudo-plateau ages are preferred when they represent internally consistent K-rich reservoirs tied to a fabric; where low-temperature steps yield younger apparent ages, or where hump-shaped spectra indicate discrete younger components, the older coherent segments are reported separately from the younger ones. Integrated ages are used only descriptively where the spectra reveal mixed reservoirs, excess argon, recoil or partial resetting. The final classification of each age combines the textural position of the dated mineral, the shape of the age spectrum, the Ca/K and Cl/K behaviour through the heating sequence, and the statistical quality of plateau, pseudo-plateau or inverse-isochron solutions. Inverse-isochron regressions were calculated in $^{36}Ar/^{40}Ar$–$^{39}Ar/^{40}Ar$ space with uncertainties on both ratios and their analytical covariance retained, as represented by 2σ error ellipses. Arrays recognized after inspection of complex multi-reservoir data are explicitly labelled exploratory and post hoc, with exact selections and sensitivity tests reported in Supplementary Table S2; they are not used as preferred age anchors.

We distinguish three levels of age interpretation: anchor ages, supported by replicated plateaux or statistically acceptable isochrons and direct textural control; corroborative ages, consistent with an independently established event but affected by partial resetting or reservoir mixing; and illustrative components, which overlap a known event but are not used quantitatively because of excess argon, large uncertainty or disturbed spectra.

4. Results

We present the results in three steps: recurrent analytical features across the dataset; the chlorine, calcium and potassium systematics that discriminate reservoirs; and the sample-by-sample results, following the north–south transect. All ages are reported with 2σ uncertainties. Analytical parameters, step-heating data, plateau and inverse-isochron calculations and preferred-age criteria are summarized in Table 2 and in the supplementary analytical tables. Complete step-heating spectra for all analysed grains and the corresponding inverse isochrons are presented in Figs. S1 and S2, respectively.

4.1 General behaviour of the spectra

The analyzed minerals do not define a single, uniform pattern. Most spectra show some disturbance in the first heating steps, commonly marked by low gas release, variable K/Ca ratios, non-chronological apparent ages and young low-temperature tails. These steps are

Table 2. Preferred $^{40}Ar/^{39}Ar$ ages, northeastern Carajás Province.

Sample	**Unit / locality**	**Mineral**	**Textural setting**	**Preferred age (Ma)**	**Method**	**MSWD / n**	**Interpretation**
Group 1: Polyphase Neoarchean hydrothermal amphibole; preferred ca. 2.52 Ga reservoir							
FT-009C	Luanga Complex	Hbl-actinolite	Cl-rich relict hydrothermal infill, subsequently stretched	2517 ± 12	Inverse isochron	1.4 / 11	Principal ca. 2.52 Ga reservoir; older and younger corroborative components
SV-01	Serra Verde garimpo	Amphibole	Undeformed syntaxial hydrothermal vein	2516 ± 14	Wtd. mean of plateau steps	0.31 / 7	Principal ca. 2.52 Ga reservoir; probable ca. 2.61 Ga initial growth
Group 2: Rhyacian (Transamazonian) fabric							
FT-049C	Parauapebas Fm.	Hornblende	Cl-poor amphibole in main foliation	2078 ± 15	Inverse isochron	1.3 / 28	Rhyacian recrystallization of main fabric
FT-087B	Parauapebas Fm.	Biotite	Fresh biotite in main foliation	2075 ± 14	Plateau	0.7 / 6	Rhyacian closure of fabric-forming reservoir
FT-193	Vila Santa Fé Cpx / Rio Preto granulite	Hornblende	Coarse high-grade schistosity	2047 ± 16	Inverse isochron	1.5 / 21	Rhyacian recrystallization/cooling, high-grade N domain
FT-024B	Cruzadão Metagranite	Biotite	Reworked basement foliation	2060 ± 10	Combined pseudo-plateau population	0.3 / 2	Rhyacian recrystallization of basement fabric
Group 3: Early Orosirian (Sereno) event							
FT-167A	Rio Novo Group	Anthophyllite–tremolite	Boudinaged fabric near shear zone	2009 ± 19	Wtd. mean of replicated plateaus	0.2 / 2	Sereno recrystallization (high-T climax)
FT-024B	Cruzadão Metagranite	Biotite	Reworked basement foliation	1965 ± 11	Combined pseudo-plateau population	3.0 / 5	Sereno recrystallization (intermediate T)
FT-078	Igarapé Cigarra succession	Muscovite	Mica fabric + crenulation	1930 ± 10	Plateau segment	4.1 / 11	Sereno mica fabric; minimum constraint (partial reset toward 1.88 Ga)
FT-138J	Águas Claras Fm. (Serra Pelada)	White mica	Slaty cleavage + crenulation	1932–1912	Plateau / pseudo-plateau cluster (4 grains)	3.5 / 4	Sereno mica fabric; minimum constraint (partial reset toward 1.88 Ga)
Group 4: ca. 1.88 Ga Uatumã components							
FT-078	Igarapé Cigarra succession	Muscovite	Sericitized domains	1877 ± 11	Pseudo-plateau	1.7 / 8	Uatumã-related hydrothermal component
FT-138J	Águas Claras Fm. (Serra Pelada)	White mica	Disturbed/altered reservoir	1876 ± 17	Pseudo-plateau	2.1 / 7	Uatumã-related hydrothermal disturbance

Notes: All ages are quoted at 2σ and include the uncertainty in J. Neutron flux monitor: Fish Canyon sanidine = 28.201 Ma; atmospheric $^{40}Ar/^{36}Ar$ = 298.56. In the MSWD / n column, n denotes isochron points, plateau steps or replicated grains according to the method listed in the adjacent column; the full step selections, initial $^{40}Ar/^{36}Ar$ values and regression statistics are given in Supplementary Table S2.

interpreted as low-retentivity or altered domains, recoil-affected releases, or minor late disturbances, and are not used in preferred-age calculations unless they form part of a coherent reservoir. In white mica and altered biotite some low-temperature steps yield Neoproterozoic apparent ages, locally near ca. 0.75 Ga, and in a few cases still younger apparent ages. These are reported as disturbed components and not as crystallization or regional ages.

The amphibole spectra show two main behaviours. Some anthophyllite and calcic amphibole grains yield relatively flat spectra or coherent plateau segments, with limited K/Ca variation and reproducible ages between replicate grains; where these minerals are texturally tied to a fabric, such ages are retained as robust recrystallization or resetting ages. Other amphiboles, especially hornblende from hydrothermally affected rocks, yield saddle-shaped spectra with anomalously old high-temperature steps. In these cases, apparent plateau ages are not used, inverse isochron ages are preferred where trapped-Ar variation is sufficient, and the result is evaluated together with the initial $^{40}Ar/^{36}Ar$ ratio and the Ca/K and Cl/K behaviour.

4.2 Chlorine, calcium and potassium components

The Cl/K and Ca/K systematics discriminate the amphibole reservoirs more sharply than the age spectra alone (Fig. 4), especially in calcic amphiboles. Grains from the hydrothermal reference assemblages carry a distinct chlorine signature. Hornblende–actinolite from the Luanga Complex (FT-009C) has elevated Cl/K, whereas hornblende that defines the main foliation in the Parauapebas Formation (FT-049C) and in the high-grade northern granulite (FT-193) has Cl/K values close to zero. Amphibole from the Parauapebas greenschist–amphibolite FT-087B, although hosted in a foliated rock, carries one of the highest Cl/K values of any analyzed amphibole, grouping it chemically with the hydrothermal reservoirs instead of the fabric-forming amphiboles. This chemical distinction is used below to interpret the origin of the amphibole in FT-087B.

The chlorine data also constrain the origin of the excess ^{40}Ar. In the hydrothermal amphibole FT-009C, apparent $^{40}Ar/^{39}Ar$ correlates strongly and positively with Cl/K, indicating that the excess ^{40}Ar is hosted in a Cl-bearing fluid component and is not distributed uniformly through the lattice. In the fabric-forming amphiboles FT-049C and FT-193, by contrast, the excess ^{40}Ar shows little or no correlation with Cl/K. This contrast is important for data reduction, as it indicates that the excess-Ar component in the fabric-forming amphiboles is less strongly coupled to a chlorine-rich fluid phase, so that their inverse-isochron intercepts are less likely to be biased by heterogeneous fluid-hosted argon.

4.3 FT-193: hornblende, Vila Santa Fé Complex (high-grade northern domain)

Sample FT-193 is a mafic granulite of the Vila Santa Fé Complex (Rio Preto mafic granulite) near the Carajás–Bacajá boundary. Its foliation is marked by oriented intergrowths of plagioclase, amphibole and pyroxene (Fig. 2b). Regional Pb–Pb zircon ages indicate a protolith near ca. 2.6 Ga, and local U–Pb zircon geochronology records high-grade metamorphism at 2069 ± 7 Ma (Tavares and Silva, 2015). The analyzed high-Ti hornblende belongs to the coarse metamorphic paragenesis and is aligned with the main schistosity, providing the highest-temperature amphibole record in the transect. Two grains show a Ca-rich reservoir (K/Ca near 0.01), low Cl/K and saddle-shaped spectra with anomalously old low-temperature steps. Plateau-like segments are older than the preferred solution and are not adopted. An inverse isochron gives 2047 ± 16 Ma (MSWD = 1.5), with a non-atmospheric initial $^{40}Ar/^{36}Ar$ confirming excess argon. This is the preferred hornblende age for the coarse high-grade schistosity (Figs. 3a, 5a, 6a).

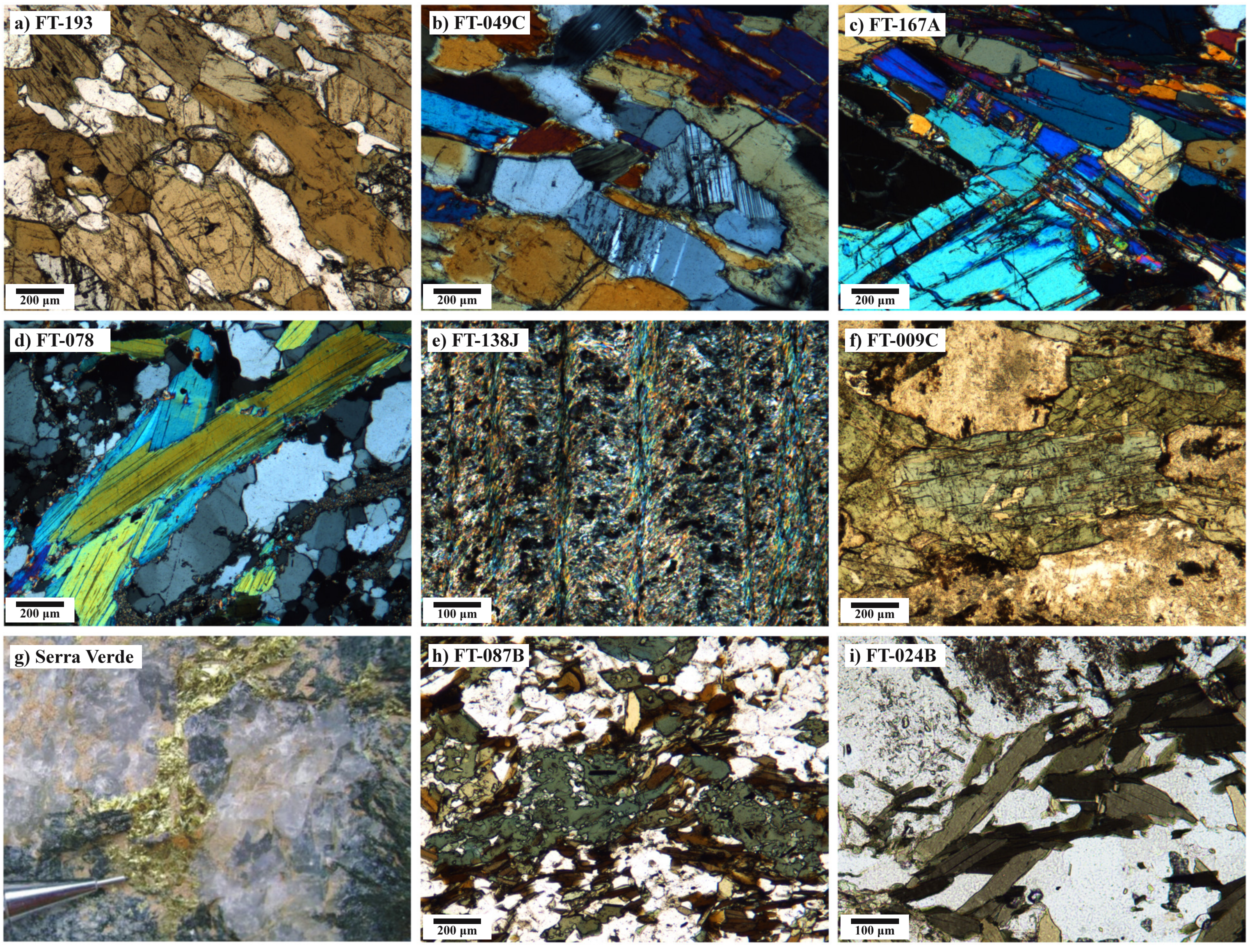

Figure 3. Photomicrographs and field detail of dated minerals and hydrothermal assemblages (PPL, plane-polarized light; XPL, crossed polarizers; scale bars as indicated). (a) FT-193, high-Ti hornblende in the coarse schistosity of the Rio Preto mafic granulite (PPL). (b) FT-049C, hornblende defining the main amphibolite foliation with plagioclase (XPL). (c) FT-167A, boudinaged anthophyllite–tremolite of the metamorphic amphibole fabric (XPL). (d) FT-078, muscovite defining the mica fabric with quartz and partial sericitization (XPL). (e) FT-138J, white mica in crenulated slaty cleavage (XPL). (f) FT-009C, optically zoned hydrothermal hornblende–actinolite from a relict coarse infill texture subsequently stretched (PPL). (g) Serra Verde vein containing stably intergrown quartz, amphibole and chalcopyrite. (h) FT-087B, amphibole partly replaced by biotite, both aligned in the main foliation (PPL). (i) FT-024B, recrystallized biotite defining the gneissic fabric with polygonal arcs (PPL).

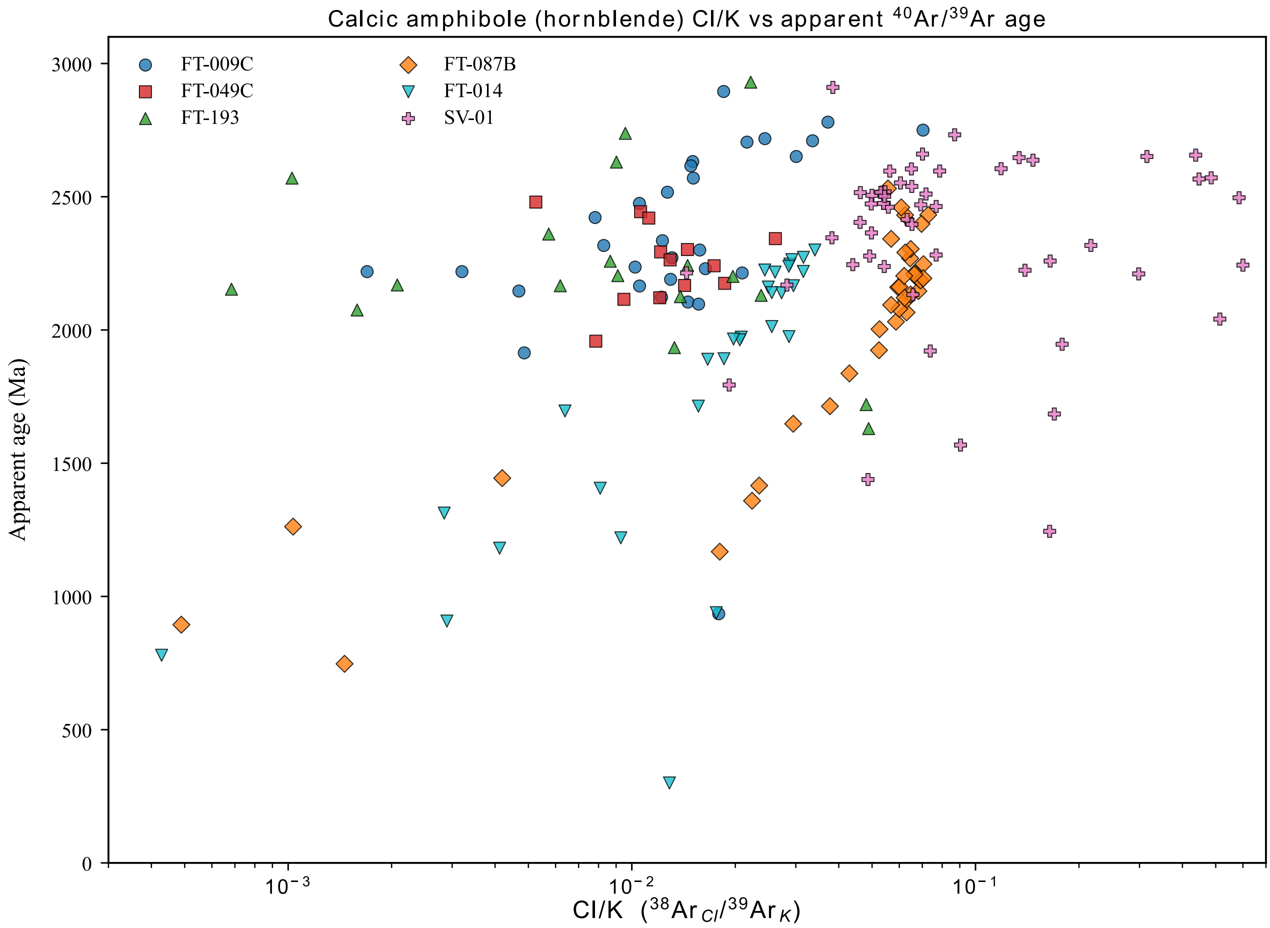

Figure 4. Chlorine systematics of the calcic amphiboles: Cl/K ($^{38}Ar\_Cl/^{39}Ar\_K$) versus apparent $^{40}Ar/^{39}Ar$ step age, coloured by sample. Fabric-forming hornblendes (FT-049C, -193, -014) have low Cl/K and apparent ages essentially uncorrelated with it, whereas the hydrothermal and inherited amphiboles (FT-009C, -087B and SV-01) have elevated Cl/K; a positive age–Cl/K correlation, clearest in FT-009C and FT-087B, supports a fluid-hosted excess-^{40}Ar component.

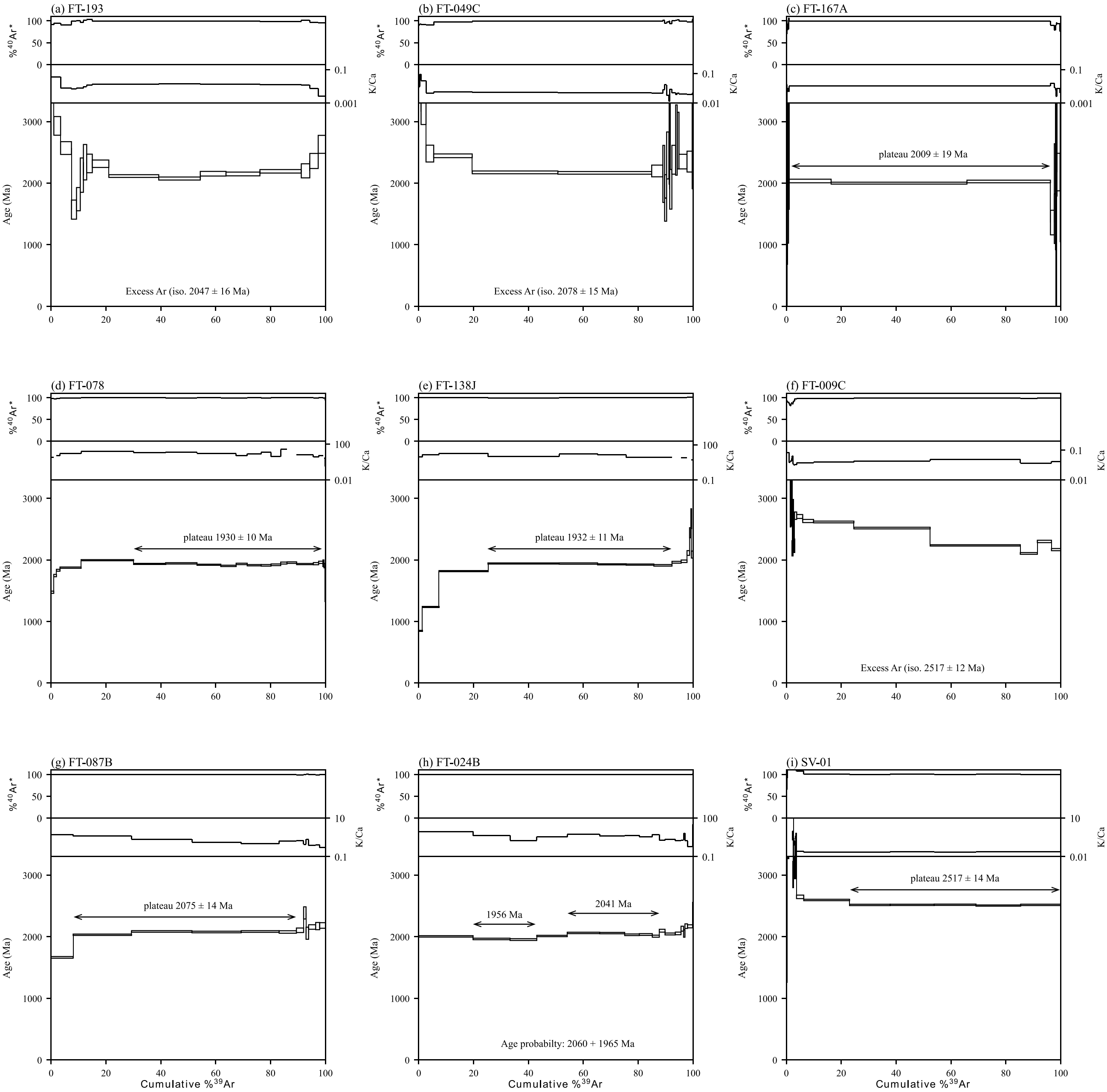

Figure 5. Representative $^{40}Ar/^{39}Ar$ step-heating spectra (complete data for all grains in Fig. S1). Each panel shows, versus cumulative % ^{39}Ar released: % $^{40}Ar^*$ (top), K/Ca (middle, log scale) and apparent age (bottom; boxes are ±2σ). (a) FT-193 and (b) FT-049C, saddle-shaped, excess-Ar hornblende (preferred inverse-isochron ages in Fig. 6). (c) FT-167A, anthophyllite–tremolite plateau. (d) FT-078 and (e) FT-138J, white-mica plateaux. (f) FT-009C, hydrothermal hornblende–actinolite (inverse isochron, Fig. 6). (g) FT-087B, fresh biotite plateau. (h) FT-024B, biotite with two pseudo-plateau populations (Fig. 7). (i) Serra Verde-01, hydrothermal amphibole plateau. Panels are ordered as cited in the text; preferred ages (Ma, 2σ) are given on the plots and in Table 2. Annotated ages are the preferred sample ages (Table 2).

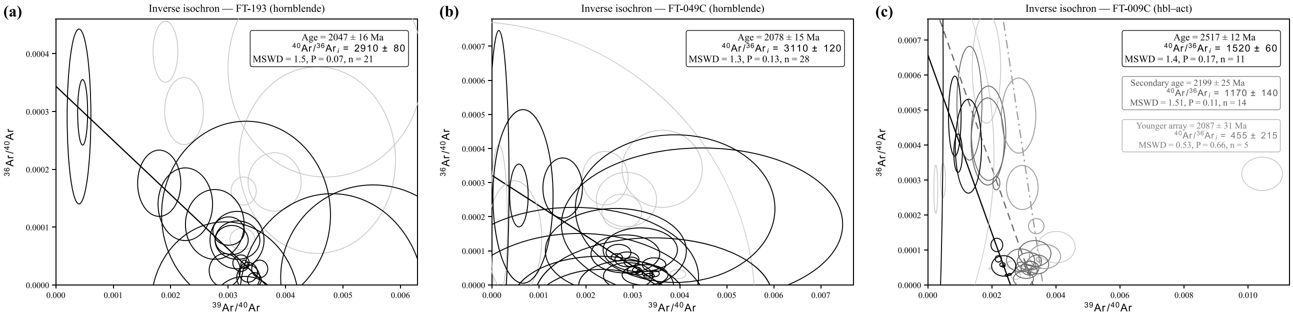

Figure 6. Inverse-isochron diagrams ($^{36}Ar/^{40}Ar$ versus $^{39}Ar/^{40}Ar$) for the excess-argon amphiboles. (a) FT-193. (b) FT-049C. (c) FT-009C. Black solid regressions and ellipses identify the preferred fits; grey ellipses are excluded. In panel (c), the dark-grey dashed regression is the 2199 ± 25 Ma secondary array defined by 8249-01G, H, K and R and 8249-02B, G–J, L and N–Q. The light-grey dash-dot regression is the 2087 ± 31 Ma younger array defined by 8249-01J, L and S and 8249-02D and K. Ages and ellipses are quoted at 2σ. Initial $^{40}Ar/^{36}Ar$ ratios, MSWD, p, n and exact step selections are given in Supplementary Table S2.

4.4 FT-049C: hornblende, Parauapebas Formation (main foliation)

Sample FT-049C is an amphibolite of the Parauapebas Formation, in the lowermost Itacaiúnas Supergroup (host volcanism ca. 2.76–2.73 Ga). The dated hornblende occurs within the main penetrative fabric. Two grains show relatively constant K/Ca (around 0.02) and Cl/K close to zero. The first steps are anomalously old and excluded; the main portions of both spectra are saddle-shaped, with old apparent ages indicating excess ^{40}Ar. Sufficient ^{36}Ar variation allows an inverse isochron at 2078 ± 15 Ma (MSWD = 1.3), with a non-atmospheric initial $^{40}Ar/^{36}Ar$. The textural link between hornblende and the penetrative fabric, together with the low Cl/K, allows us to consider this the preferred age for the main amphibolite fabric (Figs. 3b, 5b, 6b).

4.5 FT-167A: anthophyllite–tremolite, Rio Novo Group (multiple deformation phases)

Sample 4049-FT-R-167A is an anthophyllite–tremolite schist from the Rio Novo Group (host ≥ ca. 2.76 Ga), collected north of the Cigano Granite. The metamorphic amphibole fabric is defined by stable intergrowths of anthophyllite and tremolite that form a continuous schistosity but are locally boudinaged, with talc in boudin necks and microfractures indicating localized replacement during a younger deformation stage; the outcrop lies close to a ductile-brittle thrust front that crosscuts the main foliation. Two grains show simple argon-release behaviour, with coherent K/Ca (near 0.02) and flat to gently stepped spectra. Grain 1 yields a plateau age of 2010 ± 20 Ma and grain 2 a plateau age of 2000 ± 40 Ma; the combined probability distribution gives a weighted mean of 2009 ± 19 Ma. No valid inverse isochron could be calculated because the steps provide insufficient ^{36}Ar variation. The replicated plateaux, constant K/Ca and textural relation to boudinaged amphiboles justify considering 2009 ± 19 Ma as the preferred age for this sample, recording recrystallization of the amphibole during late-stage, ductile-brittle deformation (Figs. 2c, 3c, 5c, 7a). The nearby

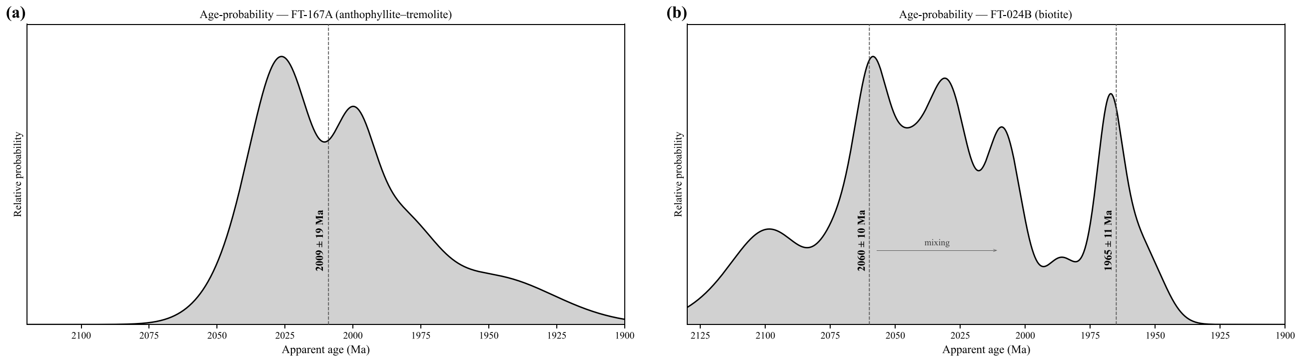

Figure 7. Relative-probability (ideogram) diagrams: (a) FT-167A anthophyllite–tremolite, a single coherent population at 2009 ± 19 Ma; (b) FT-024B biotite, two coherent populations at 2060 ± 10 Ma and 1965 ± 11 Ma (the excess-Ar high-temperature steps are excluded). Curves are the summed Gaussian probability of the selected steps; dashed lines mark the preferred ages.

FT-166 outcrop illustrates the pronounced down-dip stretching lineation in this structural domain.

4.6 FT-078: muscovite, Igarapé Cigarra succession (mica fabric)

Sample FT-078 is a sillimanite–muscovite–quartz schist from the Serra da Bocaina/Igarapé Cigarra succession (host < 2.76, > 2.73 Ga). The rock preserves two mica-bearing fabrics: an older slaty to schistose cleavage defined by muscovite and quartz, overprinted by a spaced crenulation cleavage in whose hinges muscovite forms polygonal arcs, indicating mica recrystallization during folding; some domains are partially transformed to sericite. Two muscovite grains were analyzed, with K/Ca generally between about 3 and 13. Grain 1 yields a plateau age of 1930 ± 10 Ma; its most coherent plateau segment is centered at ca. 1.93 Ga, with older apparent ages near ca. 2.0 Ga in the first steps. Grain 2 yields a reproducible pseudo-plateau of 1877 ± 11 Ma over about 40% of the released ^{39}Ar. The 1930 ± 10 Ma age is interpreted as a minimum constraint on mica recrystallization/crenulation; the 1877 ± 11 Ma pseudo-plateau is reported separately as a younger component associated with sericitized domains (Figs. 2d, 3d, 5d).

4.7 FT-138J: white mica, Águas Claras Formation (low-grade fabric)

Sample FT-138J consists of white-mica + quartz aggregates from phyllites of the lowermost Águas Claras Formation, close to the Serra Pelada artisanal mine (deposition < 2.10, > 2.00 Ga). The dated micas define a slaty cleavage locally affected by coaxial, progressive crenulation, with mica-rich domains in fold hinges. Four white-mica + quartz grains were analyzed. All spectra are hump-shaped: apparent ages rise through the low-temperature steps, flatten in the middle-temperature portion, and decline slightly at high temperature. The mid-temperature portions define coherent older segments with plateau or pseudo-plateau ages of 1932 ± 11, 1923 ± 14, 1915 ± 15 and 1912 ± 12 Ma, and a younger pseudo-plateau of 1876

± 17 Ma is also resolved; the youngest low-temperature steps yield disturbed fractions from which an isochron of approximately 250 ± 30 Ma is obtained. Because the high-temperature steps decline through the final heating steps, no older reservoir is masked beneath the ca. 1.93 Ga segments; the reproducible 1932–1912 Ma cluster is therefore interpreted as a minimum constraint on (re)crystallization of the white-mica cleavage, and the discretely resolved 1876 ± 17 Ma component as a younger, texturally distinct overprint. The ca. 250 Ma disturbed-fraction isochron and the young low-temperature steps document late disturbed argon reservoirs but are not adopted as preferred geological ages (Figs. 2e, f, 3e, 5e).

4.8 FT-009C: hornblende–actinolite, hydrothermal pocket in the Luanga Complex

Sample FT-009C was collected from a coarse amphibole–plagioclase hydrothermal pocket hosted by metagabbros of the Luanga Complex. In plan view, both the host metagabbro and the hydrothermal pockets preserve apparently primary textures, and amphibole and plagioclase form a coarse interlocking assemblage (Fig. 2g). In vertical sections parallel to the regional stretching direction, however, both the host rock and the hydrothermal aggregate display conspicuous elongation (Fig. 2h). The original texture was therefore stretched along the regional lineation, and the coarse interlocking fabric is interpreted as a relict hydrothermal infill texture.

In thin section, the amphiboles are optically heterogeneous. Darker-green internal domains are surrounded by rims with distinctly paler pleochroism. These lighter domains are interpreted as amphibole overgrowths or partially re-equilibrated original crystal margins (Fig. 3f).

The two analyzed hornblende–actinolite grains yield strongly disturbed, saddle-shaped spectra with anomalously old apparent ages and elevated Cl/K. K/Ca remains comparatively restricted through much of the principal gas-release interval, indicating that the age variation is not primarily caused by degassing of markedly different K- and Ca-bearing mineral phases. In contrast, apparent age correlates positively with Cl/K, and the oldest apparent steps are generally among the most Cl-rich. This relationship indicates that the anomalously old apparent ages are largely controlled by variable proportions of a Cl-associated trapped or excess-^{40}Ar component.

Because the spectra do not define a reliable plateau, the preferred result is the inverse isochron calculated from 11 analyses with sufficient variation in trapped argon. The regression gives an age of 2517 ± 12 Ma, an initial $^{40}Ar/^{36}Ar$ ratio of 1520 ± 60 and an MSWD of 1.4. The non-atmospheric intercept confirms excess argon and supports interpretation of the isochron age as the principal fluid-assisted amphibole-growth or isotopic re-equilibration age (Figs. 5f, 6c; Table 2).

Grain 8249-01 nevertheless preserves a systematic compositional progression through its principal high-temperature release sequence. Steps M–P yield apparent ages between 2718 ± 60 and 2616 ± 14 Ma, with relatively lower K/Ca and higher Cl/K, whereas steps Q–R have higher K/Ca, lower Cl/K and younger apparent ages of 2517 ± 13 and 2236 ± 11 Ma. This is consistent with degassing of compositionally distinct but related amphibole domains and may correspond to the observed optical zoning, although step heating provides no direct spatial correlation between gas-release steps and crystal domains. The darker internal amphibole may preserve an older, more Cl-bearing reservoir, whereas the paler rim may have grown or re-equilibrated more completely during the ca. 2.52 Ga event.

The significant steps at 2632 ± 25 and 2616 ± 14 Ma, together with other old high-temperature fractions, suggest that the hydrothermal pocket may have formed initially at ca. 2.6 Ga. These steps also lie within the mixing array that defines the 2517 Ma inverse isochron and are not treated as an independently resolved crystallization age. Apparent ages substantially older than ca. 2.6 Ga are interpreted mainly as the result of increasing contributions from Cl-associated excess argon.

Analyses excluded from the preferred inverse isochron define a secondary trend reproduced independently in both grains, with exploratory regressions of 2200 ± 24 Ma for grain 8249-01 and 2199 ± 44 Ma for grain 8249-02. A combined regression of 14 analyses gives 2199 ± 25 Ma, an initial $^{40}Ar/^{36}Ar$ ratio of 1170 ± 140, an MSWD of 1.51 and p = 0.11. The agreement between the separate grain regressions supports a genuine ca. 2.20 Ga secondary Ar component. Both regressions are sensitive to high-leverage analyses and are therefore treated as secondary mixing or re-equilibration arrays indicating selective fluid-assisted disturbance of part of the amphibole without complete resetting of the older reservoirs.

A third, younger exploratory inverse-isochron array is defined by steps J, L and S of grain 8249-01 and steps D and K of grain 8249-02. The five-point regression yields 2087 ± 31 Ma, an initial $^{40}Ar/^{36}Ar$ ratio of 455 ± 215, an MSWD of 0.53 and p = 0.66. The regression remains essentially unchanged when the comparatively imprecise step 8249-02K is omitted. It cannot be reproduced as a well-constrained independent isochron within each grain and is therefore treated as a corroborative younger array.

The analyses defining this younger array are less affected by the strongly Cl-associated excess-Ar reservoir that controls the anomalously old fractions. Their occurrence in a hydrothermal pocket conspicuously stretched along the regional lineation is consistent with limited recrystallization or isotopic re-equilibration of a less Cl-rich amphibole domain during deformation. The age therefore constrains the stretching-related modification of the hydrothermal body, although the correspondence between the regressed steps and specific recrystallized microdomains remains inferential. A few steps near ca. 2.10–2.04 Ga may record the same partial recrystallization but define no plateau or independent isochron.

FT-009C thus preserves a polyphase record: probable initial formation of the amphibole–plagioclase pocket at ca. 2.6 Ga, major fluid-assisted amphibole growth or isotopic re-equilibration at 2517 ± 12 Ma, selective re-equilibration near ca. 2.20 Ga, and a younger, comparatively low-excess-Ar component at 2087 ± 31 Ma plausibly associated with stretching.

4.9 SV-01: amphibole from an undeformed hydrothermal vein, Serra Verde

Sample SV-01 was obtained from coarse, centimetre-scale amphibole crystals in a syntaxial hydrothermal vein at the Serra Verde artisanal mine. Field relations show stable intergrowths of quartz, amphibole and chalcopyrite in the vein paragenesis (Fig. 3g), together with local association and intergrowth of amphibole and molybdenite. No visible stretching, foliation or other evidence of crystallization under directional stress was observed in the coarse-grained zones. The sample is therefore treated as an undeformed hydrothermal reference, in contrast to the subsequently stretched FT-009C pocket.

Four amphibole grains were analyzed. The first low-temperature steps generally released little gas and locally yielded unreliable ^{36}Ar measurements, peak suppression, anomalous radiogenic-Ar proportions and variable K/Ca. These fractions are not used to define preferred ages. The higher-temperature portions are more radiogenic and chemically coherent. Grain 1966-01 yields a plateau age of 2517 ± 14 Ma from steps Y–ZC, comprising approximately 77% of the released ^{39}Ar. Grain 1966-04 yields a plateau age of 2510 ± 20 Ma from steps C–D, comprising approximately 85% of the released ^{39}Ar. The weighted mean of the seven selected plateau steps is 2516 ± 14 Ma (MSWD = 0.31, p = 0.96), retained as the preferred age of the younger hydrothermal amphibole reservoir (Fig. 5i).

The spectra also preserve reproducible evidence of an older component near the local molybdenite age. Step X of grain 1966-01 yields 2596 ± 11 Ma and accounts for approximately 17% of that grain's ^{39}Ar, whereas step M of grain 1966-02 yields 2604 ± 10 Ma and accounts for approximately 24% of the gas released from that grain. Both overlap the 2609 ± 13 Ma Re–Os molybdenite age from Serra Verde (Marschik et al., 2005). Their occurrence in separate grains and their substantial gas fractions indicate that the ca. 2.60 Ga signal is not restricted to an analytically unstable, low-gas fraction.

Grain 1966-02 provides the clearest evidence of progressive isotopic re-equilibration. Steps M–O, which together account for approximately 79% of the released ^{39}Ar, decrease from 2604 ± 10 through 2552 ± 11 to 2539 ± 9 Ma while maintaining nearly invariant K/Ca values of approximately 0.021 and similar Cl/K values of 0.060–0.065. The age progression cannot be readily attributed to degassing of different mineral phases. It is consistent with compositionally similar amphibole domains that experienced different degrees of fluid-assisted isotopic re-equilibration.

The local textural association between coarse amphibole and molybdenite, together with the independently reproduced ca. 2.60 Ga steps, supports initial amphibole growth during the

2609 ± 13 Ma Cu–Mo mineralizing stage. The dominant ca. 2.52 Ga plateaux are interpreted as younger amphibole growth or extensive hydrothermal recrystallization of that pre-existing assemblage. The preferred 2516 ± 14 Ma age therefore dates the principal preserved amphibole reservoir but may postdate initial vein formation and its molybdenite-bearing paragenesis.

Grain 1966-03 contains a minor disturbed tail between ca. 2.25 and 2.13 Ga, including steps at 2169 ± 26 and 2133 ± 52 Ma. These fractions account for less than 8% of the released ^{39}Ar, are not statistically coherent and do not define a plateau or independent isochron. No robust ca. 2.10 Ga component is resolved. The absence of a coherent younger recrystallization age is consistent with the lack of visible deformation or stretching in the Serra Verde vein, although limited disturbance of small amphibole domains cannot be excluded.

Serra Verde therefore records at least two hydrothermal stages within the same coarse amphibole assemblage: probable initial growth with molybdenite at ca. 2.61 Ga, followed by extensive amphibole growth or isotopic re-equilibration at ca. 2.52 Ga. Unlike FT-009C, the undeformed vein preserves no significant younger fabric-related recrystallization.

4.10 FT-087B: amphibole and biotite, Parauapebas Formation

Sample FT-087B is a greenschist of the Parauapebas Formation from the southern part of the transect. The metamorphic assemblage includes hornblende–actinolite, biotite and sericitized domains; amphibole is the older, pre-tectonic phase in relation to the main foliation, locally transformed to biotite. Biotite is aligned with the main foliation, while younger fractures with pervasive sericitization and epidotization obliquely cut the fabric. This sample allows the comparison of amphibole, fresh biotite and altered biotite within the same fabric-bearing rock (Figs. 3h, 5g).

The two amphibole grains yield ascending, multi-reservoir spectra with nearly constant K/Ca (around 0.06) and, notably, one of the highest Cl/K values of any analyzed amphibole. The lowest-temperature steps include anomalously old apparent ages consistent with recoil; high-temperature fractions define old tails that rise to approximately 2.53 and 2.46 Ga, and medium-temperature segments between approximately 2.18 and 2.10 Ga form a coherent ledge. Because of the ascending shape and excess-Ar component, no amphibole plateau age is adopted, and the ca. 2.10 Ga ledge is reported as a maximum age for the resetting recorded by these grains, and 2.18 Ga as the minimum age. Two features indicate that the old high-temperature apparent ages are not random excess argon. First, they converge on the ca. 2.52 Ga inverse-isochron ages obtained from the demonstrably hydrothermal amphiboles of the Luanga Complex and Serra Verde. Second, the amphibole carries a hydrothermal chlorine signature indistinguishable from, and in fact stronger than, that of those hydrothermal amphiboles. Together these observations justify interpreting the amphibole in FT-R-087B as an inherited Neoarchean hydrothermal amphibole that was only partially reset during younger events, retaining most of its original argon reservoir.

The fresh biotite grain yields a well-defined plateau age of 2075 ± 14 Ma from a single K-rich reservoir (K/Ca near 1). This age is interpreted as the preferred age for the main foliation. Because biotite grew and recrystallized within the fabric whereas the more retentive amphibole was only partially reset, the biotite plateau simultaneously dates the fabric-forming event and the partial resetting of the inherited amphibole, without erasing the amphibole's Neoarchean origin. The sericitized biotite grain yields an irregular spectrum with apparent ages mostly between ca. 1.0 and 1.5 Ga and no plateau, consistent with phase mixing and multiple reservoirs; no preferred age is assigned to it.

4.11 FT-024B: biotite, Cruzadão Metagranite (reworked basement fabric)

Sample FT-024B is a biotite orthogneiss of the Cruzadão Metagranite, a Mesoarchean granitoid (crystallization 2874 ± 15 Ma; U–Pb zircon). The dated biotite belongs to the metamorphic paragenesis associated with the regional foliation, occurring as recrystallized flakes and polygonized arcs; at outcrop scale the gneissic fabric is refolded and locally transposed. These relations indicate that the biotite records recrystallization and partial resetting within a reworked basement fabric instead of the primary magmatic crystallization. Two grains show broadly similar spectra dominated by a single K-rich reservoir (K/Ca between about 2 and 10) and each contains two internally coherent pseudo-plateau segments: grain 1 yields 2041 ± 18 and 1956 ± 19 Ma, and grain 2 yields 2060 ± 30 and 1969 ± 13 Ma. A combined probability plot defines peaks at 2060 ± 10 and 1965 ± 11 Ma, while intermediate steps are considered as minimum ages for the first recrystallization event. No valid inverse isochron could be calculated because of insufficient ^{36}Ar variation. The two populations are interpreted as preferred biotite ages, recording partial resetting or recrystallization of biotite within a polyphase basement fabric during two Paleoproterozoic events (Figs. 3i, 5h, 7b).

4.12 Summary of preferred ages

The preferred results define four principal chronological and textural groups (Table 2). The first is a polyphase Neoarchean hydrothermal amphibole record, with probable initial growth at ca. 2.61–2.60 Ga and principal surviving reservoirs at 2517 ± 12 Ma in FT-009C and 2516 ± 14 Ma in SV-01; the inherited FT-087B amphibole belongs to the same archive, although its original age is not resolved. FT-009C also yields corroborative, nonpreferred arrays at

2199 ± 25 and 2087 ± 31 Ma (Table 3). The second comprises Rhyacian Transamazonian ages from the main foliation or high-grade assemblages: 2078 ± 15, 2075 ± 14, 2060 ± 10 and 2047 ± 16 Ma in FT-049C, FT-087B, FT-024B and FT-193 respectively. The third comprises Early Orosirian Sereno ages: 2009 ± 19 Ma in FT-167A and 1965 ± 11 Ma in the younger FT-024B biotite, with white mica at ca. 1.93 Ga as a minimum constraint. The fourth comprises ca. 1.88 Ga Uatumã components at 1877 ± 11 Ma in FT-078 and 1876 ± 17 Ma in FT-138J.

4.13 Non-anchor samples

Five additional samples were analyzed but are not used to anchor the Paleoproterozoic interpretation, because they preserve mixed reservoirs, large uncertainties or dominant later disturbance; their full spectra are given in the Supplementary Material. Hornblende from the Xingu amphibolite (FT-014) yields ascending, multi-reservoir spectra between a Neoproterozoic low-temperature tail and ca. 2.2–2.3 Ga, with no valid isochron; intergrown hornblende and K-feldspar from the Estrela metagranite (FT-018) yield mixed ca. 2.63 Ga and ca. 0.8 Ga components; biotite from the Rio Novo schist (FT-025A) yields ca. 1.96–1.90 Ga components reset toward ca. 1.85 Ga; muscovite from the graphite schist (FT-053) is dominated by a ca. 98 Ma isochron; and tremolite from the Rio Novo schist (FT-339B) gives a high-uncertainty ca. 2.84 Ga errorchron. These are interpreted collectively as a thermal archive in Section 5.7 (Fig. S3).

5. Discussion

5.1 What a fabric- and fluid-constrained $^{40}Ar/^{39}Ar$ age dates in Carajás

The results show that the $^{40}Ar/^{39}Ar$ record of the northeastern Carajás Province is not a set of simple cooling ages but a structured archive of recrystallization, hydrothermal growth, excess argon and partial resetting. The geological meaning of each age depends primarily on

Table 3. The thermal archive of the northeastern Carajás Province recorded by the $^{40}Ar/^{39}Ar$ dataset.

Event / age	**$^{40}Ar/^{39}Ar$ record (sample, component)**	**Independent anchor**	**Status**
Mesoarchean metamorphism (~2.84 Ga)	FT-339B tremolite errorchron ~2.84 Ga; FT-014 high-T steps (incomplete reset, to ~2.3 Ga)	Rio Novo greenstone ~2.97 Ga; Xingu Complex ~2.85 Ga	Illustrative (large error; Cl-hosted excess Ar)
Polyphase Neoarchean hydrothermalism (~2.61–2.52 Ga)	SV-01 2596 ± 11 and 2604 ± 10 Ma fractions; preferred 2516 ± 14 Ma. FT-009C ca. 2.6 Ga fractions; preferred 2517 ± 12 Ma. FT-087B inherited amphibole.	Serra Verde molybdenite 2609 ± 13 Ma; Neoarchean IOCG alteration 2.71–2.54 Ga	Preferred ca. 2.52 Ga anchors; ca. 2.61–2.60 Ga corroboration
Selective thermal–fluid re-equilibration (~2.20–2.15 Ga)	FT-009C secondary array 2199 ± 25 Ma; FT-087B and FT-014 irregular amphibole components	Corta Goela biotite 2193 ± 4 Ma (Pollard et al., 2019); Sossego amphibole 2199 ± 13 Ma (Marschik et al., 2003); Antas North titanite 2162.9 ± 28.1 Ma (Hühn et al., 2025)	Corroboration; localized fluid-assisted re-equilibration
Rhyacian – Transamazonian (2.08–2.05 Ga)	FT-049C; FT-087B biotite; FT-024B older biotite; FT-193; FT-009C younger array 2087 ± 31 Ma	Carajás–Bacajá collision (Tavares et al., 2018)	Anchor (core); FT-009C corroboration
Early Orosirian – Sereno (2.01–1.96 Ga)	FT-167A 2009; FT-024B younger biotite 1965; FT-014 grain-2 echo ~1.96	Pium (Renne et al., 1988); Jacareacanga (Vasquez et al., 2019); Guiana (Fraga et al., 2024)	Anchor (core)
Uatumã (~1.88 Ga)	FT-078 and FT-138J younger mica; FT-025A reset; Marschik et al. (2003) XB99448 K-rich ca. 1.90–1.86 Ga domains	Uatumã SLIP (1.89–1.87 Ga)	Anchor (young component)
Neoproterozoic – Araguaia (~0.8–0.75 Ga)	Mica low-T steps ~0.75 Ga; FT-018 K-feldspar ~0.8 Ga	Araguaia basin opening	Corroboration
Mesozoic disturbance (~250–98 Ma)	FT-138J errorchron ~250 Ma; FT-053 ~98 Ma	Mafic dikes cutting the units (Teixeira et al., 2019; Giovanardi et al., 2019)	Corroboration

the textural and chemical context of the dated mineral, and the chlorine and calcium systematics provide an independent test of that assignment. The same numerical interval can therefore contain several geological processes: ca. 2.61–2.52 Ga amphibole components in Cu-bearing assemblages date polyphase Archean hydrothermal growth and re-equilibration; a ca. 2.08 Ga hornblende or biotite age in the main foliation dates Rhyacian fabric recrystallization; a ca. 1.96 Ga biotite age in a reworked basement foliation dates a younger reworking event; and a ca. 1.88 Ga mica component dates hydrothermal resetting. Previous compilations that grouped all Paleoproterozoic ages in a single "Transamazonian" envelope, or read all ca. 2.00–1.90 Ga ages as Transamazonian-cooling/Uatumã mixtures, could not resolve this sequence, which emerges only when the dated minerals are placed in their tectonic and hydrothermal context.

One methodological caution must be stated explicitly. Because argon in amphibole and mica is reset mainly by recrystallization rather than by volume diffusion (Villa, 2016; Montemagni and Villa, 2025), the Paleoproterozoic ages reported here are attributed to formation of the main foliation not on the strength of the ages alone but on the independent structural evidence that this foliation overprints and transposes older Archean fabrics and affects Mesoarchean granitoids and Neoarchean supracrustal rocks alike (Tavares et al., 2018). What the argon data add is the timing of the recrystallization that accompanied that deformation.

5.2 Polyphase Neoarchean hydrothermal systems and their chlorine fingerprint

The hydrothermal amphiboles do not record a single ca. 2.52 Ga crystallization event. FT-009C and SV-01 preserve polyphase histories in which the preferred ca. 2.52 Ga ages date the principal surviving amphibole reservoir but may postdate initial formation of the hydrothermal assemblages (Figs. 5f, i, 6c).

At Serra Verde, amphibole is texturally associated and locally intergrown with molybdenite dated at 2609 ± 13 Ma, and two substantial fractions from separate grains overlap that Re–Os age, supporting initial amphibole growth during the ca. 2.61 Ga Cu–Mo mineralizing stage. The dominant ca. 2.52 Ga plateaux record younger amphibole growth or extensive fluid-assisted recrystallization of the pre-existing vein assemblage. Nearly invariant K/Ca and Cl/K through the 2604–2539 Ma sequence in grain 1966-02 indicate progressive isotopic re-equilibration within compositionally similar amphibole domains.

FT-009C preserves a comparable but structurally more complex history. Field relations identify the sampled material as a coarse amphibole–plagioclase hydrothermal infill subsequently stretched along the regional lineation (Figs. 2g, h). Significant high-temperature steps near ca. 2.6 Ga suggest initial formation of the pocket, although they define no independent age, and the preferred inverse isochron at 2517 ± 12 Ma dates major amphibole growth or isotopic re-equilibration. The optical transition from darker internal amphibole to paler rims may correspond to the change from low-K/Ca, high-Cl/K steps M–P to higher-K/Ca, lower-Cl/K steps Q–R.

Chlorine distinguishes inherited age information from spurious old apparent ages. In FT-009C, apparent age increases with Cl/K and the preferred inverse isochron has a strongly non-atmospheric initial $^{40}Ar/^{36}Ar$ ratio, so apparent ages substantially older than ca. 2.6 Ga are attributed chiefly to a Cl-associated trapped or excess-^{40}Ar reservoir. The ca. 2.6 Ga fractions may retain information on initial hydrothermal growth, whereas much older fractions primarily track fluid-hosted excess Ar. The low-Cl, age–Cl-decoupled hornblendes that define the main foliation in FT-049C and FT-193 provide an internal contrast and strengthen their Rhyacian inverse-isochron ages.

FT-009C also records two Paleoproterozoic reorganizations: a secondary array reproduced in both grains at 2199 ± 25 Ma, recording selective fluid-assisted re-equilibration without complete destruction of the Neoarchean reservoirs, and a younger five-point array at 2087 ± 31 Ma, less affected by the Cl-associated excess-Ar component and consistent with limited amphibole recrystallization during stretching. Neither is a preferred age anchor, because both were identified post hoc within a complex multi-reservoir dataset and the younger array cannot be reproduced independently within each grain.

The contrast between the two hydrothermal bodies shows that preservation of Archean Ar reservoirs depends on domain-scale recrystallization. The undeformed Serra Verde vein preserves the ca. 2.61 and 2.52 Ga stages but no coherent ca. 2.10 Ga component, whereas the stretched FT-009C body preserves the older reservoirs while also recording ca. 2.20 Ga re-equilibration and ca. 2.09 Ga deformation-related recrystallization.

The inherited high-temperature reservoir in FT-087B belongs in this broader context. Its elevated Cl/K and old apparent ages identify a Neoarchean hydrothermal amphibole, but the data do not require original crystallization specifically at ca. 2.52 Ga. The amphibole preserves an older Cl-bearing hydrothermal reservoir that was only partially re-equilibrated during Paleoproterozoic fabric development.

5.3 Rhyacian (re)crystallization and the age of the main regional foliation

The Rhyacian ages are 2078 ± 15 Ma in hornblende from FT-049C, 2075 ± 14 Ma in biotite from FT-087B, 2060 ± 10 Ma in the older biotite population of FT-024B, and 2047 ± 16 Ma in hornblende from FT-193. Because biotite recrystallizes readily within a fabric and its spectra are least affected by excess argon, we treat biotite as the primary chronometer and the excess-Ar-corrected amphiboles as corroboration. The two Parauapebas Formation anchors are the key ties: a hornblende inverse-isochron age of 2078 ± 15 Ma from the main amphibolite fabric in FT-049C, and a 2075 ± 14 Ma biotite plateau from fresh biotite in the main foliation in FT-087B. These indistinguishable ages, from minerals with different retention behaviour, indicate that the main foliation in a typical Neoarchean supracrustal unit recrystallized in the Rhyacian.

The older biotite population of FT-024B extends this result into the Mesoarchean basement. The sample is a biotite orthogneiss of the ca. 2.87 Ga Cruzadão Metagranite in which biotite defines a transposed, refolded fabric; the 2060 ± 10 Ma population dates recrystallization within a reworked basement foliation. This is important because it shows that the Paleoproterozoic fabric was not restricted to supracrustal sequences but also reworked Mesoarchean granitoids, tens of kilometers to the south of the suture between Carajás and Bacajá.

The high-grade northern sample FT-193 provides a further constraint. Its 2047 ± 16 Ma hornblende age is younger than the 2069 ± 7 Ma zircon U–Pb age of high-grade metamorphism reported for the same rock (Tavares and Silva, 2015), consistent with recrystallization or cooling of hornblende after the metamorphic peak. The northern, high-grade hornblende is thus younger than the southern hornblende and biotite at ca. 2.08 Ga, the expected sense for a northward-increasing metamorphic gradient in which hotter, deeper northern rocks remained above the amphibole retention window longer. This inference is suggestive only, because the two ages barely separate at the 2σ level and FT-193 is an excess-Ar isochron age.

Together these ages provide the thermochronological counterpart to the structural interpretation of Tavares et al. (2018). Field relations had already indicated that the first penetrative fabric affecting Neoarchean supracrustal rocks and reworking Mesoarchean basement in northeastern Carajás was Paleoproterozoic; the argon data now date the minerals that crystallized or recrystallized within that fabric. The main foliation preserved in major Archean host units of the province is therefore not an inherited Neoarchean fabric but records Rhyacian activity of a Paleoproterozoic tectono-metamorphic architecture (Fig. 8c).

FT-009C provides a complementary constraint from a pre-existing hydrothermal body. Its younger exploratory inverse-isochron array at 2087 ± 31 Ma overlaps the preferred fabric-forming amphibole and biotite ages, while field sections show that the original amphibole–plagioclase infill was stretched along the regional Transamazonian lineation (Figs. 2g, h, 6c). The five-analysis array cannot be reproduced independently within each grain and is not an age anchor. Its agreement with the structural position nevertheless corroborates ca. 2.08 Ga reworking and partial recrystallization of an older hydrothermal body.

5.4 The Early Orosirian Sereno event (ca. 2.01–1.96 Ga)

The second Paleoproterozoic signal is defined by two fabric-forming minerals of contrasting retentivity. Anthophyllite–tremolite from FT-167A yields replicated plateaux averaging 2009 ± 19 Ma and provides the northernmost anchor: its boudinaged, talc-bearing grains record recrystallization during localized deformation near a Sereno shear zone. Biotite from the reworked basement gneiss FT-R-024B yields 1965 ± 11 Ma within the same rock that preserves the ca. 2.06 Ga Rhyacian population, direct evidence that the younger event reworked basement anisotropies as well as supracrustal fabrics. Both are younger than the Rhyacian group and older than the ca. 1.88 Ga Uatumã components, bracketing an Early Orosirian interval that cannot be reduced to analytical mixing between the two.

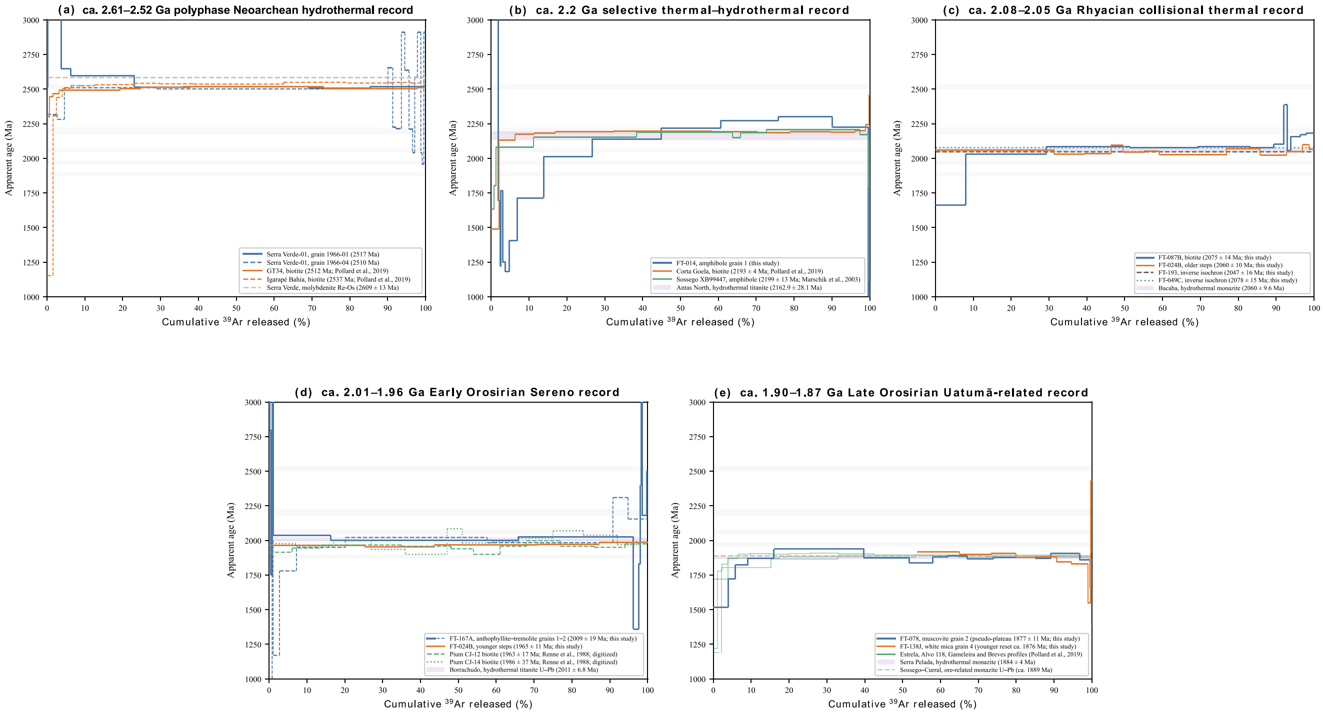

Figure 8. Event-based synthesis of selected $^{40}Ar/^{39}Ar$ spectra from this study and published regional constraints (Ar-Ar, Re-Os, U-Pb), plotted against cumulative ^{39}Ar released on a common age scale. Grey horizontal bands mark the principal age windows discussed in the text. (a) Dominant ca. 2.61-2.52 Ga Neoarchean hydrothermal reservoir in SV-01 and regional comparisons. (b) ca. 2.20 Ga selective thermal–hydrothermal record in FT-014 and published constraints (c) ca. 2.08–2.05 Ga Rhyacian collisional record, including the older FT-024B biotite population. (d) ca. 2.01–1.96 Ga Early Orosirian Sereno record, including the younger FT-024B population and regional comparisons. (e) ca. 1.90–1.87 Ga late Orosirian Uatumã-related record, with FT-078 grain 2, FT-138J grain 4 and published constraints. Spectra from this study, Marschik et al. (2003) and Pollard et al. (2019) were reconstructed from tabulated data; spectra from Renne et al. (1988) were digitized from published figures. Quoted summary ages retain the published values.

This interval stands on a firm footing beyond the present transect. Flat biotite spectra of 1963 ± 17 and 1986 ± 37 Ma from the Pium Complex (Renne et al., 1988) fall squarely within it, and at the Borrachudo copper deposit a U–Pb titanite age of 2011 ± 6.8 Ma dates an albite–chalcopyrite–apatite vein (Previato et al., 2020). Coeval early Orosirian tectonism is widespread: in the Tapajós Domain, high-grade metamorphism and syn-foliation leucogranite anatexis in the Jacareacanga Group are dated at ca. 1.95 Ga (1946 ± 14 to 1956 ± 27 Ma; Vasquez et al., 2019), and the central Guiana Shield preserves early Orosirian belts of comparable age (Fraga et al., 2024). The Sereno event is therefore one regional expression of a craton-scale ca. 2.0–1.95 Ga reworking of Rhyacian crust.

The low-grade mica fabrics record this event only as a minimum. The main foliation at Serra Pelada is structurally part of the Sereno architecture, yet white mica from FT-138J (1932–1912 Ma) and muscovite from FT-078 (1930 ± 10 Ma) yield ca. 1.93 Ga, below the ca. 1.96 Ga of the fresh anchors. Both lie within the hydrothermal footprint of the Serra Pelada deposit: their thin sections show sericitized muscovite and sillimanite, their spectra resolve a discrete ca. 1.88 Ga component (1877 ± 11 and 1876 ± 17 Ma), and FT-138J carries a ca. 250 Ma disturbed fraction. Their younger apparent ages track proximity to that hydrothermal system rather than a distinct 1.93 Ga event or a contrast in retentivity: biotite in FT-024B, away from the deposit, retained 1965 Ma, whereas the more retentive muscovite within the footprint did not, consistent with recrystallization-controlled argon behaviour in micas (Villa, 2016; Montemagni and Villa, 2025). The most retentive muscovite steps in FT-078 still preserve apparent ages near 2.0 Ga. We therefore treat the mica ages as a corroborating floor. Structurally, this Early Orosirian pulse corresponds to the Sereno event of the regional mapping. The combination of regionally effective deformation with limited fluid-assisted recrystallization (a relatively low-temperature, fluid-limited pulse) explains why the event is subtle in high-temperature systems and why it is best resolved by fabric-constrained analysis of intermediate- to low-retentivity minerals. The overall Paleoproterozoic record is thus episodic: at least two recrystallization events (Rhyacian and Sereno) followed by localized late Orosirian hydrothermal resetting (Fig. 8d).

5.5 The ca. 1.88 Ga Uatumã overprint and younger disturbances

The ca. 1.88 Ga components in FT-078 (1877 ± 11 Ma) and FT-138J (1876 ± 17 Ma) are best interpreted as the argon expression of the Uatumã-related magmatic–hydrothermal system. In both samples these ages occur in low-retentivity or sericitized mica reservoirs, coexist with older coherent segments, and are not tied to a new penetrative regional foliation. This is consistent with the role of Uatumã as late Orosirian anorogenic magmatism and granite-related hydrothermal circulation, strongest in micas and altered domains where partial recrystallization generates young pseudo-plateaux (Fig. 8e).

The lowest-temperature steps of several samples additionally record younger, weaker thermal disturbances. Neoproterozoic apparent ages near ca. 0.6–0.8 Ga, and Mesozoic apparent ages near ca. 0.15–0.25 Ga obtained mostly from disturbed fractions, are consistent respectively with reactivation related to the opening and inversion of the Araguaia basin and with Mesozoic reactivation recorded by regional mafic dyke swarms (Giovanardi et al., 2019; Teixeira et al., 2019; Cruz and Gorayeb, 2020).

5.6 Re-reading Paleoproterozoic ages in Carajás and the eastern Amazonian Craton

The event-based reading refines both older regional data and the geochronological-province model. The ca. 2.20 Ga signal is resolved within the present dataset and not supported only by regional comparisons: the secondary FT-009C arrays described above are reproduced in both grains and indicate a common secondary Ar reservoir.

This component overlaps the 2193 ± 4 Ma Corta Goela biotite age and the dominant 2199 ± 13 Ma amphibole reservoir at Sossego–Sequeirinho, while the 2162.9 ± 28.1 Ma hydrothermal-titanite age from Antas North extends the interval toward ca. 2.15 Ga (Marschik et al., 2003; Pollard et al., 2019; Hühn et al., 2025; Fig. 8b), together defining a regionally reproducible ca. 2.20–2.15 Ga thermal–fluid episode. The Sossego–Sequeirinho result is broadly understood as a minimum age for the grains (e.g. Moreto et al., 2015a), with primary amphibole growth more plausibly associated with the ca. 2.71–2.68 Ga alteration and mineralizing system; its ca. 2.20 Ga reservoir can instead record substantial but incomplete Paleoproterozoic re-equilibration. The absence of reported Cl/K data precludes testing the role of excess Ar in the older fractions.

We distinguish the ca. 2.20–2.15 Ga selective fluid-assisted episode from the younger ca. 2.10–2.08 Ga recrystallization associated with deformation and stretching, coeval with other biotite and amphibole ages from this study. The latter is represented by the 2087 ± 31 Ma FT-009C array and by the 2.09–2.11 Ga fractions of amphiboles described by Marschik et al. (2003) at Sossego–Sequeirinho. The contrasting structural expression supports successive stages of selective fluid-mediated re-equilibration followed by more effective deformation-related recrystallization of inherited amphibole.

The distinct Sereno event also has implications beyond Carajás. Early Orosirian ages near 2.01–1.96 Ga overlap deformation, metamorphism and syn-tectonic magmatism in neighbouring Amazonian domains, including Tapajós and the central Guiana Shield (Fraga et al., 2024). In the Amapá Block, Transamazonian amphibole ages of 2087 ± 3 to 2047 ± 20 Ma and biotite ages of 2079 ± 18 to 2033 ± 13 Ma are indistinguishable from the Rhyacian ages reported here, whereas the Carecuru Domain records younger biotite at 1928 ± 19 and

1833 ± 13 Ma (Rosa-Costa et al., 2009). Near-identical amphibole–biotite ages across two segments of the craton reinforce the regional coherence of the Rhyacian signal.

5.7 The full thermal archive: from Mesoarchean metamorphism to Mesozoic rifting

The anchors of this study occupy a narrow Paleoproterozoic window, but the dataset preserves a much longer record. Disturbed, mixed and partially reset spectra are treated as informative only where an internally coherent component coincides with an independently dated event, and as illustrative where large uncertainties or excess argon prevent a quantitative interpretation. Under these criteria, the archive extends from a ca. 2.84 Ga tremolite errorchron in FT-339B to Mesozoic disturbance (Table 3; Fig. 9).

The contrast between two chronometers in reworked Mesoarchean basement illustrates the mechanism. Biotite in the Cruzadão orthogneiss FT-024B recrystallized readily and resolves Rhyacian and Sereno populations at 2060 ± 10 and 1965 ± 11 Ma. Hornblende in the Xingu amphibolite FT-014 recorded the same history less completely: its coherent gas is almost entirely radiogenic, precluding an isochron, and apparent ages rise from a Neoproterozoic tail through a Sereno segment to ca. 2.2–2.3 Ga, recording incomplete Paleoproterozoic re-equilibration of older amphibole complicated by Cl-hosted excess argon.

Preservation of Archean amphibole reservoirs was not restricted to undeformed or low-strain rocks. As described in Section 5.2, the undeformed Serra Verde vein and the conspicuously stretched FT-009C pocket both retain their Neoarchean reservoirs, and only the stretched body adds the younger ca. 2.20 and 2.09 Ga components. Penetrative deformation did not erase the Archean record where recrystallization remained spatially restricted: older domains survived beside newly grown or re-equilibrated ones.

Thermal archive of NE Carajás — $^{40}Ar/^{39}Ar$ record from the Mesoarchean to the Mesozoic

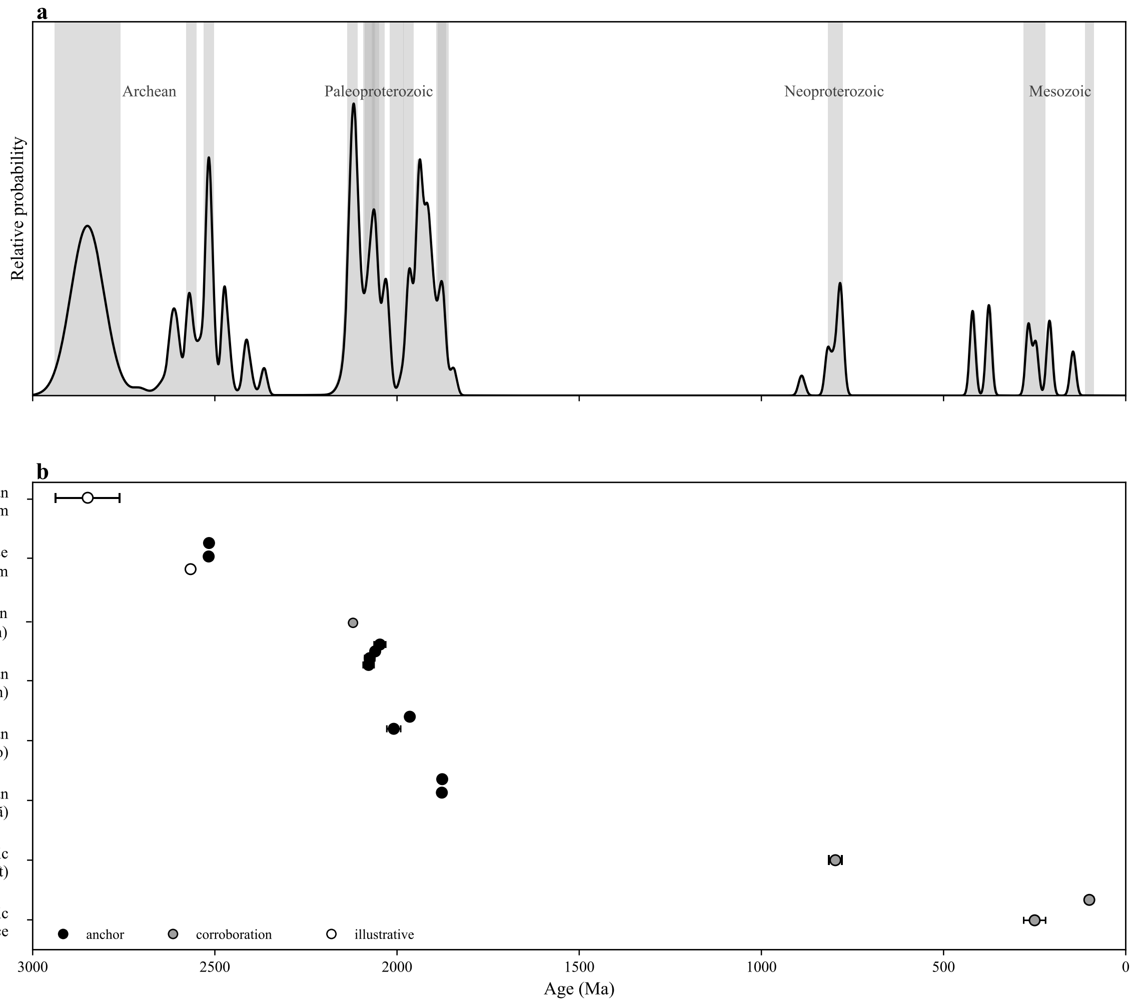

Figure 9. Thermal archive of the northeastern Carajás Province from the Mesoarchean to the Mesozoic. (a) Relative-probability distribution of step ages contributing to interpreted components, plus Araguaia and Mesozoic disturbance steps; grey bars mark anchor ages. (b) Components grouped by event and confidence: anchor (filled black), corroboration (grey) and illustrative (open).

At the young end of the archive, low-temperature mica steps and K-feldspar in the Estrela metagranite (FT-018) record Neoproterozoic disturbance broadly coeval with the opening of the Araguaia basin and Brasiliano reactivation. An errorchron near 250 Ma in FT-138J and a ca. 98 Ma isochron in FT-053 coincide broadly with Mesozoic mafic dikes that cut the units (Teixeira et al., 2019; Giovanardi et al., 2019). These components define no regional fabrics, but they extend the resolved thermal record by more than 1.7 Gyr beyond its Paleoproterozoic core.

6. Conclusions

Fabric- and fluid-constrained $^{40}Ar/^{39}Ar$ geochronology calibrates the polycyclic tectonic architecture of the northeastern Carajás Province. Minerals recrystallized within the main regional fabrics record a Rhyacian Transamazonian event at ca. 2.08–2.05 Ga and an Early Orosirian Sereno event at ca. 2.01–1.96 Ga. White mica near Serra Pelada provides ca. 1.93 Ga minimum constraints partially reset toward a ca. 1.88 Ga Uatumã overprint. These ages date recrystallization of mapped fabrics in Archean host rocks, not host-rock formation.

Hydrothermal amphiboles preserve a polyphase Neoarchean record. At Serra Verde, substantial fractions at 2596 ± 11 and 2604 ± 10 Ma overlap the 2609 ± 13 Ma Re–Os molybdenite age and support initial amphibole growth during Cu–Mo mineralization. The dominant 2516 ± 14 Ma reservoir records younger growth or extensive hydrothermal recrystallization. FT-009C similarly preserves evidence consistent with initial formation of its amphibole–plagioclase pocket at ca. 2.6 Ga, whereas the preferred 2517 ± 12 Ma inverse isochron dates the principal subsequent fluid-assisted growth or re-equilibration. Cl/K systematics show that substantially older apparent ages chiefly reflect variable contributions from a Cl-associated trapped or excess-^{40}Ar reservoir.

The northeastern Carajás Province is therefore an Archean crustal block repeatedly reworked during the Paleoproterozoic. Its argon record is a domain-scale archive of hydrothermal growth, excess-Ar trapping, selective fluid-mediated re-equilibration and deformation-assisted recrystallization. Linking each age to mineral chemistry, microstructure and regional fabric separates discrete tectonic and hydrothermal events within a broad Paleoproterozoic age envelope and provides a transferable strategy for other polycyclic cratons.

Acknowledgements

We thank the staff of the Argon Geochronology in Earth Sciences laboratory (UQ-AGES), School of the Environment, The University of Queensland, for training, laboratory access and analytical support throughout the 40Ar/39Ar work. We especially thank Benjamin E. Cohen for helping with sample preparation and for reading and commenting an earlier version of the manuscript. F.M.T. thanks the Geological Survey of Brazil (SGB/CPRM) for institutional and logistical support during fieldwork and sampling in the Carajás Province, and the Programa de Pós-Graduação em Geologia of the Universidade Federal do Rio de Janeiro (UFRJ), where this study was developed as part of his doctoral research. The authors thank colleagues at SGB/CPRM and UFRJ for discussions that improved the interpretations presented here, and Farid Chemale Jr. for his careful reading and constructive comments on an earlier version of the manuscript.

CRediT authorship contribution statement

Felipe Mattos Tavares: Conceptualization, Investigation (sampling, mineral selection and petrography), Formal analysis (40Ar/39Ar data reduction, analytical quality control and age calculations), Visualization (figures and tables), Writing – original draft, Project administration. Rudolph Allard Johannes Trouw: Supervision, Writing – review & editing.

Paulo Marcos Vasconcelos: Methodology, Investigation (sample preparation, mineral separation, irradiation and 40Ar/39Ar analyses; sampling of the Serra Verde reference), Resources (UQ-AGES argon geochronology laboratory), Writing – review & editing.

Funding

This study was carried out as part of the doctoral research of F.M.T., supported by a doctoral scholarship from the Coordenação de Aperfeiçoamento de Pessoal de Nível Superior (CAPES). Fieldwork, sampling and related activities in the Carajás Province were funded by the Geological Survey of Brazil (SGB/CPRM). The 40Ar/39Ar analyses were performed at the UQ-AGES argon geochronology laboratory, The University of Queensland, with analytical support from the laboratory.

Declaration of competing interest

The authors declare that they have no known competing financial interests or personal relationships that could have appeared to influence the work reported in this paper.

Data availability

The primary analytical data and source data underlying the figures are openly available in Mendeley Data at https://doi.org/10.17632/dgc4gn89ry.1. Revised age calculations, exact step selections for preferred and exploratory arrays, and interpretive metadata are provided in the Supplementary Data Package submitted with this article. Supplementary figures and explanatory material are also provided with the article. Original laboratory files are available from the corresponding author upon reasonable request.

Declaration of generative AI and AI-assisted technologies in the manuscript preparation process

During the preparation of this work, the authors used OpenAI’s ChatGPT and Anthropic’s Claude to assist with language editing, the organization and development of the manuscript text, data processing and consistency checks, and the layout of figures and tables. Assistance with figures was limited to composition, labelling and the plotting of diagrams derived directly from the analytical data. No generative AI tool was used to create, modify, enhance or otherwise alter any image representing primary observed data, including the photomicrographs in Figs. 3 and S3, and no generative AI tool was used to produce the primary analytical data. All AI-assisted output was critically reviewed, verified and edited by the authors, who take full responsibility for the content of the published article.

References

Araújo, O.J.B., Maia, R.G.N., Silva, J.J.X., Costa, J.B.S., 1988. A megaestruturação da folha Serra dos Carajás. In: Congresso Latino-Americano de Geologia, 7, Belém, Anais, pp. 324–333.

Araújo, R., Nogueira, A.C.R., Araújo, R.N., 2020. New stratigraphic proposal of a Paleoproterozoic siliciclastic succession: implications for the evolution of the Carajás Basin, Amazonian Craton, Brazil. Journal of South American Earth Sciences 102, 102665.

Barbosa, J.P.O., 2004. Geologia estrutural, geoquímica, petrografia e geocronologia de granitóides da região do Igarapé Gelado, norte da Província Mineral de Carajás. MSc thesis, Universidade Federal do Pará, Belém, 112 p.

Barros, C.E.M., Macambira, M.J.B., Barbey, P., 2001. Idade de zircão do Complexo Granítico Estrela: relações entre magmatismo, deformação e metamorfismo na Província Mineral de Carajás. In: Simpósio de Geologia da Amazônia, 7, Belém, Resumos Expandidos, SBG, pp. 17–20.

Berger, G.W., 1975. $^{40}Ar/^{39}Ar$ step heating of thermally overprinted biotite, hornblende and potassium feldspar from Eldora, Colorado. Earth and Planetary Science Letters 26, 387–408.

Billström, K., Bergman, S., Mark, C., Barfod, D.N., 2025. New ^{40}Ar/^{39}Ar mineral ages of Archaean to early Proterozoic rocks in northern Sweden and implications for the 1.8–1.5 Ga tectonothermal history of northernmost Fennoscandia. International Journal of Earth Sciences 114, 347–368.

Caswell, B., Gilotti, J.A., Webb, L.E., McClelland, W.C., Kośmińska, K., Piepjohn, K., von Gosen, W., 2021. ^{40}Ar/^{39}Ar dating of Paleoproterozoic shear zones in the Ellesmere–Devon crystalline terrane, Nunavut, Canadian Arctic. Canadian Journal of Earth Sciences 58, 1073–1084.

Chagondah, G.S., Kramers, J.D., Hofmann, A., Rollinson, H., 2024. Neoarchaean and Palaeoproterozoic tectono-metamorphic events along the southern margin of the Zimbabwe Craton: insights from muscovite ^{40}Ar/^{39}Ar geochronology from rare-metal pegmatites, Zimbabwe. Journal of African Earth Sciences 217, 105333.

Cordani, U.G., 1981. Comentários sobre as determinações geocronológicas disponíveis na Folha SC.22-Tocantins. In: Projeto RADAMBRASIL, Folha SC.22-Tocantins, Rio de Janeiro, pp. 173–174.

Cordani, U.G., Brito Neves, B.B., Fuck, R.A., Porto, R., Thomaz-Filho, A., Cunha, F.M.B., 1984. Estudo preliminar de integração do Pré-Cambriano com os eventos tectônicos das bacias sedimentares brasileiras. Ciência Técnica Petróleo, Seção Exploração de Petróleo 15, 70 p.

Costa, J.B.S., Araújo, O.J.B., Santos, A., Jorge João, X.S., Macambira, M.J.B., Lafon, J.M., 1995. A Província Mineral de Carajás: aspectos tectono-estruturais, estratigráficos e geocronológicos. Boletim do Museu Paraense Emílio Goeldi, Série Ciências da Terra 7, 199–235.

Costa, U. A. P.; Paula, R. R.; Silva, D. P. B.; Barbosa, J. P. O.; Silva, C. M. G.; Tavares, F. M.; Oliveira, J. K. M.; Justo, A. P.; 2016. Mapa geológico-geofísico ARIM Carajás (versão preliminar). Belém: CPRM, 1 map, colour. 1:250.000.

Cruz, D.J.N., Gorayeb, P.S.S., 2020. Geology and petrology of the mafic dike swarms of the Araguaia Belt: evidence for distinct events of intracontinental magmatism in central-northern Brazil and correlations with large igneous provinces. Journal of South American Earth Sciences 100, 102563.

Dall'Agnol, R., Teixeira, N.P., Rämö, O.T., Moura, C.A.V., Macambira, M.J.B., Oliveira, D.C., 2005. Petrogenesis of the Paleoproterozoic, rapakivi, A-type granites of the Archean Carajás Metallogenic Province, Brazil. Lithos 80, 101–129.

Delinardo, M.A., 2014. Metatexitos e diatexitos do Complexo Xingu na região de Canaã dos Carajás: implicações para a evolução mesoarqueana do Domínio Carajás. MSc thesis, Universidade Estadual de Campinas, Campinas, 110 p.

Dodson, M.H., 1973. Closure temperature in cooling geochronological and petrological systems. Contributions to Mineralogy and Petrology 40, 259–274.

Feio, G.R.L., Dall'Agnol, R., Dantas, E.L., Macambira, M.J.B., Santos, J.O.S., Althoff, F.J., Soares, J.E.B., 2013. Archean granitoid magmatism in the Canaã dos Carajás area: implications for crustal evolution of the Carajás Province, Amazonian Craton, Brazil. Precambrian Research 227, 157–186.

Ferron, J.M.T.M., Bastos Neto, A.C., Lima, E.F., Nardi, L.V.S., Costi, H.T., Pierosan, R., Prado, M., 2010. Petrology, geochemistry, and geochronology of Paleoproterozoic volcanic and granitic rocks (1.89–1.88 Ga) of the Pitinga Province, Amazonian Craton, Brazil. Journal of South American Earth Sciences 29, 483–497.

Fleck, R.J., Sutter, J.F., Elliott, D.H., 1977. Interpretation of discordant $^{40}Ar/^{39}Ar$ age spectra of Mesozoic tholeiites from Antarctica. Geochimica et Cosmochimica Acta 41, 15–32.

Fraga, L.M., Cordani, U., Dreher, A.M., Sato, K., Reis, N.J., Nadeau, S., De Roever, E., Kroonenberg, S., Maurer, V.C., 2024. Early Orosirian belts of the central Guiana Shield, northern Amazonian Craton: U–Pb geochronology and tectonic implications. Precambrian Research 407, 107362.

Gibbs, A.K., Wirth, K.R., Hirata, W.K., Olszewski Jr., W.J., 1986. Age and composition of the Grão Pará Group volcanics, Serra dos Carajás. Revista Brasileira de Geociências 16, 201–211.

Giovanardi, T., Girardi, V.A.V., Teixeira, W., Mazzucchelli, M., 2019. Mafic dyke swarms at 1882, 535 and 200 Ma in the Carajás region, Amazonian Craton: Sr–Nd isotopy, trace element geochemistry and inferences on their origin and geological settings. Journal of South American Earth Sciences 92, 197–208.

Gomes, C.B., Cordani, U.G., Basei, M.A.S., 1975. Radiometric ages from the Serra dos Carajás area, northern Brazil. Geological Society of America Bulletin 86, 939–945.

Grainger, C.J., Groves, D.I., Tallarico, F.H.B., Fletcher, I.R., 2008. Metallogenesis of the Carajás Mineral Province, southern Amazon Craton, Brazil: varying styles of Archean through Paleoproterozoic to Neoproterozoic base- and precious-metal mineralization. Ore Geology Reviews 33, 451–489.

Grove, M., Harrison, T.M., 1996. $^{40}Ar^*$ diffusion in Fe–Mg amphiboles. Journal of Geophysical Research: Solid Earth 101, 557–572.

Harrison, T.M., 1981. Diffusion of ^{40}Ar in hornblende. Contributions to Mineralogy and Petrology 78, 324–331.

Harrison, T.M., Célérier, J., Aikman, A.B., Hermann, J., Heizler, M.T., 2009. Diffusion of ^{40}Ar in muscovite. Geochimica et Cosmochimica Acta 73, 1039–1051.

Hasui, Y., Abreu, F.A.M., Silva, J.M.R., 1977. Estratigrafia da Faixa de Dobramentos Paraguai-Araguaia no centro-norte do Brasil. Boletim do Instituto de Geociências 8, 107–118.

Holdsworth, R.E., Butler, C.A., Roberts, A.M., 1997. The recognition of reactivation during continental deformation. Journal of the Geological Society 154, 73–78.

Holdsworth, R.E., Pinheiro, R.V.L., 2000. The anatomy of shallow-crustal transpressional structures: insights from the Archaean Carajás fault zone, Amazon, Brazil. Journal of Structural Geology 22, 1105–1123.

Hühn, S.R.B., Paula, R.N., Fonseca, F.J.F., Barreira, I.B., 2025. Geology and hydrothermal evolution of the Antas North iron sulfide–copper–gold (ISCG) deposit in the Carajás Mineral Province. Minerals 15, 1081. https://doi.org/10.3390/min15101081

Kuiper, K.F., Deino, A., Hilgen, F.J., Krijgsman, W., Renne, P.R., Wijbrans, J.R., 2008. Synchronizing rock clocks of Earth history. Science 320, 500–504.

Macambira, E.M.B., Ricci, P.S.F., Anjos, G.C., 2016. Carta Geológica: folha Repartimento – SB.22-X-A. CPRM, Belém, scale 1:250,000.

Machado, N., Lindenmayer, D.H., Krogh, T.E., Lindenmayer, Z.G., 1991. U–Pb geochronology of Archean magmatism and basement reactivation in the Carajás area, Amazon Shield, Brazil. Precambrian Research 49, 329–354.

Marschik, R., Spangenberg, J.E., Leveille, R.A., de Almeida, A.J., 2003. The Sossego iron oxide Cu–Au deposit, Carajás, Brazil. In: Eliopoulos, D.G., et al. (Eds.), Mineral Exploration and Sustainable Development, vol. 1. Millpress, Rotterdam, pp. 331–334.

Marschik, R., Mathur, R., Ruiz, J., Leveille, R.A., de Almeida, A.J., 2005. Late Archean Cu–Au–Mo mineralization at Gameleira and Serra Verde, Carajás Mineral Province, Brazil: constraints from Re–Os molybdenite ages. Mineralium Deposita 39, 983–991.

Marangoanha, B., Oliveira, D.C., Dall'Agnol, R., 2019. The Archean granulite–enderbite complex of the northern Carajás Province, Amazonian Craton (Brazil): origin and implications for crustal growth and cratonization. Lithos 350–351, 105275.

McDougall, I., Harrison, T.M., 1999. Geochronology and Thermochronology by the $^{40}Ar/^{39}Ar$ Method, 2nd ed. Oxford University Press, Oxford.

Melo, G.H.C., Monteiro, L.V.S., Xavier, R.P., Moreto, C.P.N., Santiago, E.S.B., Dufrane, S.A., Aires, B., Santos, A.F.F., 2017. Temporal evolution of the giant Salobo IOCG deposit, Carajás Province (Brazil): constraints from paragenesis of hydrothermal alteration and U–Pb geochronology. Mineralium Deposita 52, 709–732.

Min, K., Mundil, R., Renne, P.R., Ludwig, K.R., 2000. A test for systematic errors in $^{40}Ar/^{39}Ar$ geochronology through comparison with U/Pb analysis of a 1.1-Ga rhyolite. Geochimica et Cosmochimica Acta 64, 73–98.

Monteiro, L.V.S., Xavier, R.P., Carvalho, E.R., Hitzman, M.W., Johnson, C.A., Souza Filho, C.R., Torresi, I., 2008. Spatial and temporal zoning of hydrothermal alteration and mineralization in the Sossego iron oxide–copper–gold deposit, Carajás Mineral Province, Brazil: paragenesis and stable isotope constraints. Mineralium Deposita 43, 129–159.

Montemagni, C., Villa, I.M., 2025. Dating deformation by the $^{40}Ar/^{39}Ar$ method: a review. Italian Journal of Geosciences 144, 250–263.

Moreto, C.P.N., Monteiro, L.V.S., Xavier, R.P., Creaser, R.A., Tassinari, C.C.G., Sato, K., Kemp, A.I.S., Amaral, W.S., 2015a. Neoarchean and Paleoproterozoic iron oxide–copper–

gold events at the Sossego deposit, Carajás Province, Brazil: Re–Os and U–Pb geochronological evidence. Economic Geology 110, 809–835.

Moreto, C.P.N., Monteiro, L.V.S., Xavier, R.P., Creaser, R.A., DuFrane, S.A., Melo, G.H.C., Delinardo da Silva, M.A., Tassinari, C.C.G., Sato, K., 2015b. Timing of multiple hydrothermal events in the iron oxide–copper–gold deposits of the Southern Copper Belt, Carajás Province, Brazil. Mineralium Deposita 50, 517–546.

Nogueira, A.C.R., Truckenbrodt, W., Pinheiro, R.V.L., 1995. Formação Águas Claras, Pré-Cambriano da Serra dos Carajás: redescrição e redefinição litoestratigráfica. Boletim do Museu Paraense Emílio Goeldi, Série Ciências da Terra 7, 177–277.

Paixão, M.A.P., Nilson, A.A., Dantas, E.L., 2008. The Neoproterozoic Quatipuru ophiolite and the Araguaia fold belt, central-northern Brazil, compared with correlatives in NW Africa. Geological Society, London, Special Publications 294, 297–318.

Pidgeon, R.T., Macambira, M.J.B., 2000. Th–U–Pb isotopic systems and internal structures of complex zircons from an enderbite from the Pium Complex, Carajás Province, Brazil. Chemical Geology 166, 159–171.

Pinheiro, R.V.L., Holdsworth, R.E., 1997. Reactivation of Archaean strike-slip fault systems, Amazon region, Brazil. Journal of the Geological Society 154, 99–103.

Pinheiro, R.V.L., Holdsworth, R.E., 2000. Evolução tectonoestratigráfica dos sistemas transcorrentes Carajás e Cinzento, Cinturão Itacaiúnas, na borda leste do Cráton Amazônico, Pará. Revista Brasileira de Geociências 30, 597–606.

Pollard, P.J., Taylor, R.G., Peters, L., Matos, F., Freitas, C., Saboia, L., Huhn, S., 2019. $^{40}Ar/^{39}Ar$ dating of Archean iron oxide Cu–Au and Paleoproterozoic granite-related Cu–Au deposits in the Carajás Mineral Province, Brazil: implications for genetic models. Mineralium Deposita 54, 329–346.

Previato, M., Monteiro, L.V.S., Bello, R.M.S., Gonçales, L.C.G., 2020. Evolution of brines and CO_2-rich fluids and hydrothermal overprinting in the genesis of the Borrachudo copper deposit, Carajás Province. Ore Geology Reviews 121, 103561.

Renne, P.R., Onstott, T.C., Jorge João, X.S., 1988. $^{40}Ar/^{39}Ar$ and paleomagnetic results from the Guaporé Shield: implications for Proterozoic mobile belts of Gondwanaland. In: Congresso Latino-Americano de Geologia, 7, Belém, Anais, v. 1, pp. 348–362.

Rosa-Costa, L.T., Monié, P., Lafon, J.-M., Arnaud, N.O., 2009. ^{40}Ar–^{39}Ar geochronology across Archean and Paleoproterozoic terranes from southeastern Guiana Shield (north of Amazonian Craton, Brazil): evidence for contrasting cooling histories. Journal of South American Earth Sciences 27, 113–128.

Santos, J.O.S., 2003. Geotectônica dos escudos das Guianas e Brasil-Central. In: Bizzi, L.A., Schobbenhaus, C., Vidotti, R.M., Gonçalves, J.H. (Eds.), Geologia, Tectônica e Recursos Minerais do Brasil. CPRM, Brasília, pp. 169–226.

Scheiber, T., Viola, G., Ganerød, M., Bingen, B., 2023. $^{40}Ar/^{39}Ar$ constraints on the tectonic evolution of the central part of the Mesoproterozoic Sveconorwegian orogen. Journal of Structural Geology 166, 104777.

Schutesky, M.E., Oliveira, C.G., 2020. The Carajás IOCG System, Brazil. Ore Geology Reviews 127, 103833.

Tavares, F.M., 2014. Programa Geologia do Brasil – PGB. Rio Verde, Folha SB.22-Z-A-III, Estado do Pará: Carta Geológica. CPRM, Belém, 1 map, colour, scale 1:100,000.

Tavares, F.M., 2015. Evolução tectônica policíclica da porção nordeste da Província Carajás, sudeste do Cráton Amazônico. Unpublished PhD thesis, Universidade Federal do Rio de Janeiro, Rio de Janeiro.

Tavares, F.M., Silva, C.M.G., 2015. Programa Geologia do Brasil – PGB. Serra Pelada, Folha SB.22-X-C-VI, Estado do Pará: Carta Geológica. CPRM, Belém, 1 map, colour, scale 1:100,000.

Tavares, F.M., Trouw, R.A.J., Silva, C.M.G., Justo, A.P., Oliveira, J.K.M., 2018. The multistage tectonic evolution of the northeastern Carajás Province, Amazonian Craton, Brazil: revealing complex structural patterns. Journal of South American Earth Sciences 88, 238–252.

[dataset] Tavares, F. M.; Trouw, R. A. J.; Vasconcelos, P. M.; Cohen, B. E., 2026. $^{40}Ar/^{39}Ar$ step-heating data and preferred-age calculations for the northeastern Carajás Province, Amazonian Craton, Mendeley Data, V1, DOI: 10.17632/dgc4gn89ry.1

Teixeira, W., Tassinari, C.C.G., Cordani, U.G., Kawashita, K., 1989. A review of the geochronology of the Amazonian Craton: tectonic implications. Precambrian Research 42, 213–227.

Teixeira, W., Hamilton, M.A., Girardi, V.A.V., Faleiros, F.M., Ernst, R.E., 2019. U–Pb baddeleyite ages of key dyke swarms in the Amazonian Craton (Carajás/Rio Maria and Rio Apa areas): tectonic implications for events at 1880, 1110 Ma, 535 Ma and 200 Ma. Precambrian Research 329, 138–155.

Trendall, A.F., Basei, M.A.S., De Laeter, J.R., Nelson, D.R., 1998. SHRIMP U–Pb constraints on the age of the Carajás Formation, Grão Pará Group, Amazon Craton. Journal of South American Earth Sciences 11, 265–277.

Trunfull, E.F., Hagemann, S.G., Xavier, R.P., Cliff, J., 2020. Critical assessment of geochronological data from the Carajás Mineral Province, Brazil: implications for metallogeny and tectonic evolution. Ore Geology Reviews. https://doi.org/10.1016/j.oregeorev.2020.103545

Vasconcelos, P.M., Onoe, A.T., Kawashita, K., Soares, A.J., Teixeira, W., 2002. $^{40}Ar/^{39}Ar$ geochronology at the Instituto de Geociências, USP: instrumentation, analytical procedures, and calibration. Anais da Academia Brasileira de Ciências 74, 297–342.

Vasquez, M.L., Rosa-Costa, L.T. (Eds.), 2008. Geologia e Recursos Minerais do Estado do Pará: SIG, texto explicativo dos mapas geológico, tectônico e de recursos minerais. CPRM, Belém.

Vasquez, M.L., Macambira, M.J.B., Armstrong, R.A., 2008. Zircon geochronology of granitoids from the western Bacajá Domain, southeastern Amazonian Craton, Brazil: Neoarchean to Orosirian evolution. Precambrian Research 161, 279–302.

Vasquez, M.L., Pinheiro, F.G.R., Rodrigues, J.B., Tavares, F.M., Faraco, M.T.L., 2019. Idades U–Pb por LA-ICP-MS em zircão das rochas do Grupo Jacareacanga, sudoeste do Domínio Tapajós. In: Simpósio de Geologia da Amazônia, 16, Manaus. SBG-NO, expanded abstract.

Villa, I.M., 2016. Diffusion in mineral geochronometers: present and absent. Chemical Geology 420, 1–10.

Wirth, K.R., Gibbs, A.K., Olszewski Jr., W.J., 1986. U–Pb ages of zircons from the Grão Pará Group and Serra dos Carajás granite, Pará, Brazil. Revista Brasileira de Geociências 16, 195–200.

Xavier, R.P., Monteiro, L.V.S., Moreto, C.P.N., Pestilho, A.L.S., Melo, G.H.C., Silva, M.A.D., Aires, B., Ribeiro, C., Freitas e Silva, F.H., 2012. The iron oxide copper–gold systems of the Carajás Mineral Province. In: Hedenquist, J.W., Harris, M., Camus, F. (Eds.), Geology and Genesis of Major Copper Deposits and Districts of the World. Society of Economic Geologists Special Publication 16, pp. 433–454.

Supplementary Material 1

Analytical procedures, data-reduction criteria and sample-level interpretation

Manuscript: Fabric- and fluid-constrained $^{40}Ar/^{39}Ar$ geochronology of the northeastern Carajás Province, Amazonian Craton: separating hydrothermalism from Rhyacian and Orosirian reworking of Archean crust

1. Data package structure

The data package (Tavares et al., 2026) contains ten sheets.

Table S1. Structure of the supplementary data package (workbook sheets and their contents).

Sheet	Content
README	Package description, calibration, Serra Verde provenance and sample-naming note.
Metadata	Irradiation parameters (J by irradiation), neutron-induced interference corrections, mass discrimination factors, decay constants, monitor age and atmospheric ratios. Reported once here rather than repeated on every analytical row.
SampleKey	Mapping between analytical-sheet sample names (unpadded, e.g. 4049-FT-49C) and manuscript names (zero-padded, e.g. 4049-FT-049C). Raw data names are unchanged.
SampleCounts	Step counts, materials and apparent-age ranges for every sample, including Serra Verde-01.
PreferredAges	Preferred ages and interpreted components used in the manuscript.
IsochronSelections	Exact FT-009C preferred, secondary and younger array selections, regression statistics, selection status and sensitivity notes.
NonAnchorSamples	The five samples documented in the supplementary spectra and excluded from the anchor set.
AnalyticalData_cleaned	Main step-heating dataset, 536 rows and 68 columns.
AnalyticalData_SerraVerde	Serra Verde-01 step-heating data, 85 rows (4 grains).
RunIndex_1966	Run-position index for the Serra Verde-01 session.

Table S2 summarizes the preferred and exploratory inverse-isochron arrays, regression statistics and exact heating-step selections. Preferred ages remain the basis of the main chronological framework; secondary arrays are reported transparently as corroborative or exploratory results.

Table S2. Preferred plateau and inverse-isochron ages and exploratory FT-009C arrays; ellipses and quoted ages are 2σ.

Sample	**Dated mineral**	**Preferred age (Ma)**	**Method**	**Steps / analyses**	**%^{39}Ar**	**$^{40}Ar/^{36}Ar_i$**	**MSWD**	**p**	**n**
Group 1. Polyphase Neoarchean hydrothermal amphibole; preferred ca. 2.52 Ga reservoir									
FT-009C	Hbl–actinolite	2517 ± 12	Inverse isochron, preferred	8249-01B, D, E, I, M–Q; 8249-02F, T	—	1520 ± 60	1.40	0.17	11
FT-009C	Hbl–actinolite	2199 ± 25	Secondary inverse-isochron array, post hoc	8249-01G, H, K, R; 8249-02B, G–J, L, N–Q	—	1170 ± 140	1.51	0.11	14
FT-009C	Hbl–actinolite	2087 ± 31	Younger inverse-isochron array, post hoc	8249-01J, L, S; 8249-02D, K	—	455 ± 215	0.53	0.66	5
SV-01	Amphibole	2516 ± 14	Wtd. mean of plateau steps	1966-01 Y–ZC; 1966-04 C–D (7 steps)	—	atmospheric	0.31	0.96	7
Group 2. Rhyacian (Transamazonian) fabric									
FT-049C	Hornblende	2078 ± 15	Inverse isochron	28 analyses	—	3110 ± 120	1.30	0.13	28
FT-087B	Biotite	2075 ± 14	Plateau	disc 8248, steps C–I (6)	~20	atmospheric	0.70	0.62	6
FT-193	Hornblende	2047 ± 16	Inverse isochron	21 analyses	—	2910 ± 80	1.50	0.07	21
FT-024B	Biotite	2060 ± 10	Wtd. mean of two grain plateaus	discs 8245-01/-02 (2 grains)	~27	atmospheric	0.30	0.58	2
Group 3. Early Orosirian (Sereno) event									
FT-167A	Anthophyllite–tremolite	2009 ± 19	Wtd. mean of replicated plateaus	discs 8256-01/-02 (2 grains)	~72	atmospheric	0.20	0.65	2
FT-024B	Biotite	1965 ± 11	Combined pseudo-plateau population	low-T steps, 2 grains (5)	~32	atmospheric	3.00	0.02	5
FT-078	Muscovite	1930 ± 10	Plateau segment	steps H–V (11)	~49	atmospheric	4.10	0.000	11
FT-138J	White mica	1932–1912	Plateau / pseudo-plateau cluster	4 grains	~49	atmospheric	3.50	0.01	4
Group 4. ca. 1.88 Ga Uatumã components									
FT-078	Muscovite	1877 ± 11	Pseudo-plateau	high-T sericitized steps (8)	~24	atmospheric	1.70	0.10	8
FT-138J	White mica	1876 ± 17	Pseudo-plateau	disturbed steps (7)	~15	atmospheric	2.10	0.05	7

2. Samples retained

The main spreadsheet contains analytical rows followed by workbook metadata. Rows were retained where the run identifier follows the analytical pattern and the sample field corresponds to a Carajás sample or a laboratory standard. The retained main extraction contains 536 rows and 68 columns. Serra Verde-01 (SV-01) adds 85 rows from a separate session (S4).

Table S3. Samples and analytical rows retained in the reduced dataset, with material and role.

Sample	Steps	Material	Role
FT-49C	38	Amphibole	Rhyacian main-fabric anchor
FT-87B	69	Amphibole; Biotite	Rhyacian biotite anchor; inherited hydrothermal amphibole
FT-193	29	Amphibole	Rhyacian high-grade northern-domain anchor
FT-24B	38	Biotite	Rhyacian and Sereno components in basement fabric
FT-167A	29	Amphibole (ath–tr)	Sereno/Early Orosirian anchor
FT-78	38	Muscovite	Sereno mica and Uatumã-related component
FT-138J	62	White mica	Sereno mica, Uatumã component and disturbed fractions
FT-009C	41	Amphibole	Polyphase hydrothermal pocket; preferred ca. 2.52 Ga and secondary ca. 2.20/2.09 Ga arrays
SV-01	85	Amphibole (hornblende)	Undeformed polyphase hydrothermal vein; ca. 2.61 and 2.52 Ga components
FT-014	42	Amphibole	Non-anchor; multiple reservoirs
FT-018	41	Amphibole + K-feldspar	Non-anchor; mixed reservoirs
FT-025A	—	Biotite	Non-anchor; supplementary support
FT-053	45	Phyllite/muscovite	Non-anchor; late disturbance
FT-339B	26	Tremolite/amphibole	Non-anchor; high uncertainty
FT-024A	30	Biotite + Quartz	Raw data only
PP-020	8	Hornblende	Standard/unknown; raw data only

3. Sample preparation and analytical procedure

Crushed material was cleaned in an ultrasonic bath with distilled water and ethanol, then dried. From each split, 20 to 50 grains of 0.5 to 2 mm were hand-picked under a binocular microscope, favoring optically clean grains from the target fabric or hydrothermal assemblage. Fresh and altered grains were separated where alteration was central to the interpretation, so that distinct argon reservoirs could be evaluated independently.

Aliquots of five to ten grains were loaded into aluminum irradiation discs with Fish Canyon sanidine flux monitors at an age of 28.201 Ma (Kuiper et al., 2008). The discs were closed with aluminum lids, wrapped in aluminum foil and vacuum heat-sealed in quartz vials. Irradiation lasted 14 h at the B-1 CLICIT facility of the Radiation Center, Oregon State University. After a decay period, two to four grains from each sample were analyzed by laser incremental $^{40}Ar/^{39}Ar$ step heating at the University of Queensland, following Vasconcelos et al. (2002). Gas released at each step was purified before isotopic measurement. Blank corrections and neutron-induced interference corrections for K- and Ca-derived argon isotopes were applied step by step, and the neutron-flux parameter J was calculated from interspersed monitors. Ages were calculated with the decay constants of Min et al. (2000) and carry 2σ uncertainties that include the uncertainty in J.

The reference sample Serra Verde-01 was analyzed in a separate, earlier session and reduced and refit by B. Cohen in 2012 (irradiation 0201-108). It uses the same Fish Canyon age (28.201 Ma) and the same atmospheric $^{40}Ar/^{36}Ar$ (298.56) as the main dataset, and its ages are directly comparable. Its 85 step-heating measurements, over four grains (runs 1966-01 to 1966-04), appear in sheet AnalyticalData_SerraVerde. In that sheet, Ar39_Moles is derived as Ar40_Moles divided by the measured $^{40}Ar/^{39}Ar$, and Pct39Ar_cum_per_grain is the cumulative ^{39}Ar fraction per grain; all other values come from the Cohen (2012) reduction.

Low-temperature steps of Serra Verde-01 have small gas amounts and locally unreliable ^{36}Ar, and the high-temperature and plateau steps are analytically robust.

4. Data-reduction and preferred-age criteria

Several analyzed minerals contain more than one argon reservoir, so ages were classified conservatively. The final interpretation of each age combines the textural position of the dated mineral, the shape of the age spectrum, the Ca/K and Cl/K behavior through the heating sequence, and the statistical quality of the plateau, pseudo-plateau or inverse-isochron solution.

The Ca/K ratio (from Ca-derived ^{37}Ar over K-derived ^{39}Ar) and the Cl/K ratio (from Cl-derived ^{38}Ar over K-derived ^{39}Ar) serve as chemical discriminators between reservoirs. Chlorine incorporation depends on crystal chemistry, so Cl/K is diagnostic in minerals able to host chlorine, principally the Fe-bearing calcic amphiboles. Low Cl/K in muscovite and in the Mg-rich anthophyllite–tremolite follows from the structure of these minerals, and carries no direct information on fluid salinity. Cl/K comparisons are therefore restricted to minerals of similar potassium content.

Table S4. Operational criteria used to classify and treat multi-reservoir argon spectra.

Feature observed	Operational treatment	Interpretive implication
Formal plateau	Retained when ≥3 contiguous steps comprise ≥50% of released ^{39}Ar and are coherent at 95% confidence.	Preferred when texturally linked to the target fabric or assemblage.
Pseudo-plateau / coherent segment	Reported when reproducible, internally coherent and consistent with petrography, and labelled as a component.	Applies to mixed mica and partially reset biotite systems.
Saddle-shaped amphibole spectrum	Inverse isochron provides the age where trapped-argon variation is sufficient; the initial ^{40}Ar/^{36}Ar evaluates excess argon.	Excess ^{40}Ar and inherited reservoirs; the geological meaning follows the textural setting.
Secondary / exploratory inverse-isochron array	Reported with exact analyses, covariance treatment, leverage/sensitivity tests and post-hoc status.	Corroborative or exploratory only; never used as a preferred age anchor.
Young low-temperature steps	Excluded from preferred ages unless they define a coherent reservoir.	Low-retentivity altered domains, recoil, and late disturbance.
Ca/K and Cl/K behavior	Used to identify phase mixing, alteration and fluid-hosted argon in K-comparable minerals.	Elevated Cl/K in Fe-bearing amphiboles marks the Neoarchean Cl-rich hydrothermal fluid.
Integrated age	Used descriptively for disturbed or multiphase spectra.	Not adopted as a preferred age.

5. Preferred ages and interpretive status

Table S5 lists the preferred ages and interpreted components used in the manuscript. Table S2 additionally reports the nonpreferred FT-009C arrays and their exact selections. Ages listed as components or minimum constraints should be read with their textural context. Serra Verde-01 is a hydrothermal reference sample, and its complete step-heating data appear in sheet AnalyticalData_SerraVerde of the data package.

Table S5. Preferred $^{40}Ar/^{39}Ar$ ages and interpretive status of each sample.

Sample	Dated mineral	Textural setting	Preferred age (Ma)	Age type	Interpretive use
FT-009C	Hornblende-actinolite	Relict coarse hydrothermal infill, subsequently stretched; Cl-rich	2517 ± 12	Inverse isochron	Principal ca. 2.52 Ga reservoir in a polyphase hydrothermal pocket
SV-01	Amphibole	Undeformed syntaxial vein; quartz–amphibole–chalcopyrite and local molybdenite	2516 ± 14	Weighted mean, plateau steps (n = 7)	Principal ca. 2.52 Ga reservoir; probable ca. 2.61 Ga initial growth
FT-049C	Hornblende	Main penetrative fabric; low Cl	2078 ± 15	Inverse isochron	Rhyacian recrystallization of main fabric
FT-087B	Biotite	Fresh biotite in main foliation	2075 ± 14	Plateau	Rhyacian closure of fabric-forming reservoir
FT-193	Hornblende	Coarse high-grade schistosity	2047 ± 16	Inverse isochron	Rhyacian recrystallization, high-grade N domain
FT-024B	Biotite	Reworked basement foliation	2060 ± 10	Combined pseudo-plateau	Rhyacian recrystallization of basement fabric
FT-167A	Anthophyllite-tremolite	Boudinaged fabric near shear zone	2009 ± 19	Weighted mean, replicated plateaux	Sereno fluid-assisted resetting
FT-024B	Biotite	Reworked basement foliation	1965 ± 11	Combined pseudo-plateau	Sereno recrystallization
FT-078	Muscovite	Mica fabric and crenulation	1930 ± 10	Plateau segment	Sereno mica recrystallization
FT-138J	White mica	Slaty cleavage and crenulation	1932–1912	Plateau/ pseudo-plateau cluster	Sereno mica recrystallization
FT-078	Muscovite	Sericitized domains	1877 ± 11	Pseudo-plateau	Uatumã-related component
FT-138J	White mica	Disturbed/altered reservoir	1876 ± 17	Pseudo-plateau	Uatumã-related disturbance

SV-01 per-grain results: grain 1966-01 plateau 2517 ± 14 Ma (steps Y–ZC, ~77% ^{39}Ar; MSWD = 0.33, p = 0.86); grain 1966-04 plateau 2510 ± 20 Ma (steps C–D, ~85% ^{39}Ar; MSWD = 0.59, p = 0.86). The preferred weighted mean of seven selected plateau steps is 2516 ± 14 Ma (MSWD = 0.31, p = 0.96). Older steps 1966-01X at 2596 ± 11 Ma and 1966-02M at 2604 ± 10 Ma overlap the 2609 ± 13 Ma Re–Os molybdenite age and support a probable older hydrothermal component. Grain 1966-02 steps M–O decrease from 2604 ± 10 to 2539 ± 9 Ma at nearly invariant K/Ca and Cl/K, consistent with progressive isotopic re-equilibration in compositionally similar amphibole domains.

6. Non-anchor samples

Five samples are documented for completeness and excluded from the anchor set. Their spectra appear in the supplementary figures.

Table S6. Non-anchor samples documented for completeness and excluded from the anchor set.

Sample	Mineral	Behavior	Reason for exclusion
FT-014	Amphibole	Pseudo-plateau segments near 2.26–2.23 Ga	Multiple reservoirs and partial resetting
FT-018	Amphibole + K-feldspar	Mixed reservoirs; 2.63 Ga and 0.80 Ga components	Phase mixing and complex argon record
FT-025A	Biotite	1.96–1.90 Ga components with 1.85 Ga resetting	Supportive of Sereno/Uatumã; less diagnostic
FT-053	Muscovite/phyllite	Mesozoic resetting, 150–250 Ma	Late thermal disturbance
FT-339B	Tremolite/amphibole	Old apparent ages with high uncertainty (2.85 ± 0.09 Ga)	High uncertainty and possible excess argon
FT-009C (secondary)	Hbl–actinolite	2199 ± 25 Ma combined array; separate grains 2200 ± 24 and 2199 ± 44 Ma	Post-hoc, leverage-sensitive array; corroborative fluid-assisted re-equilibration
FT-009C (younger)	Hbl–actinolite	2087 ± 31 Ma five-point array; stable when imprecise 8249-02K is omitted	Post-hoc and not reproducible per grain; corroborative deformation-related component

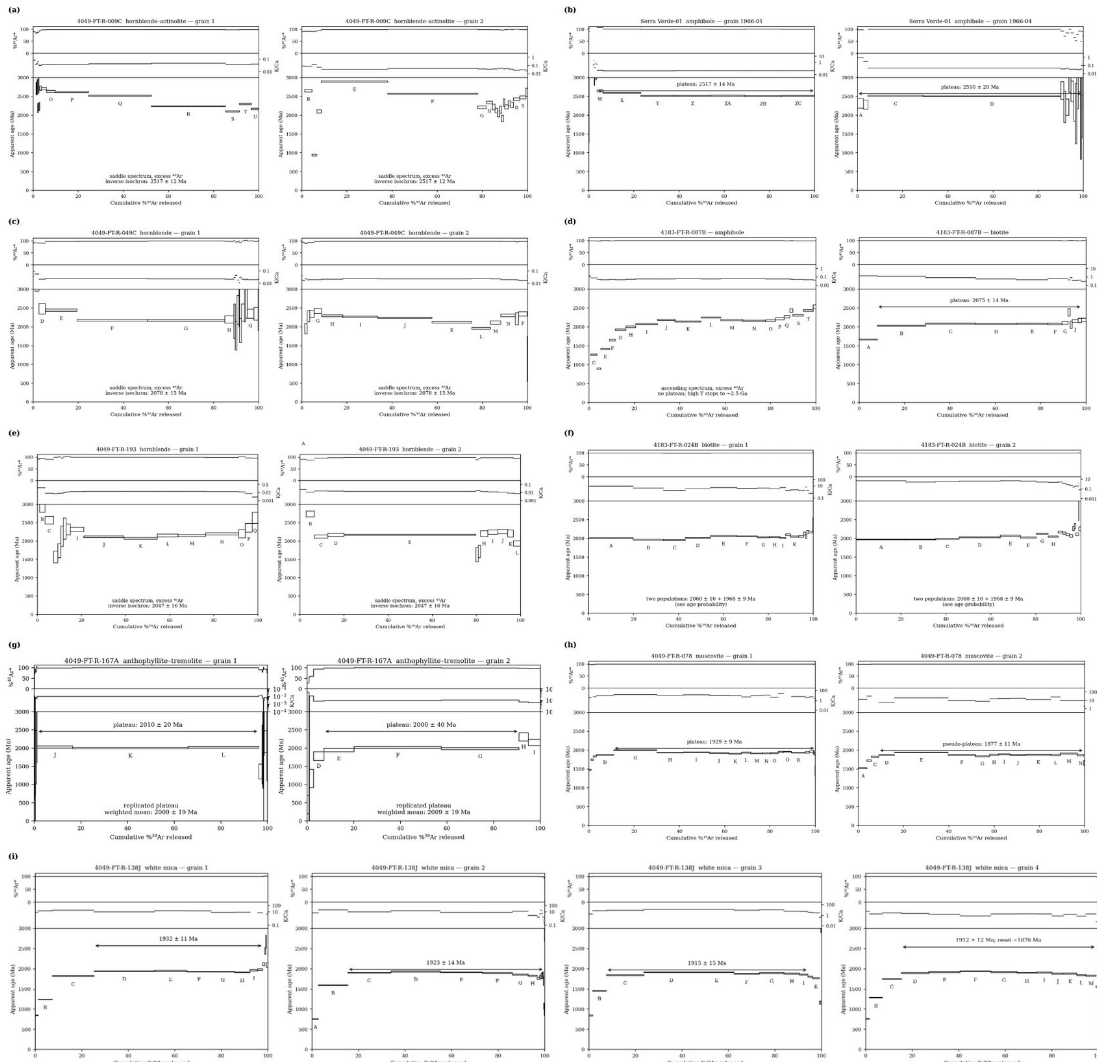

Fig. S1. Complete $^{40}Ar/^{39}Ar$ step-heating spectra for the anchor samples (two grains per sample, except FT-138J with four grains, and SV-01 with the two grains that yield preferred plateaux); non-anchor samples are shown in Fig. S3. Same conventions as Fig. 5.

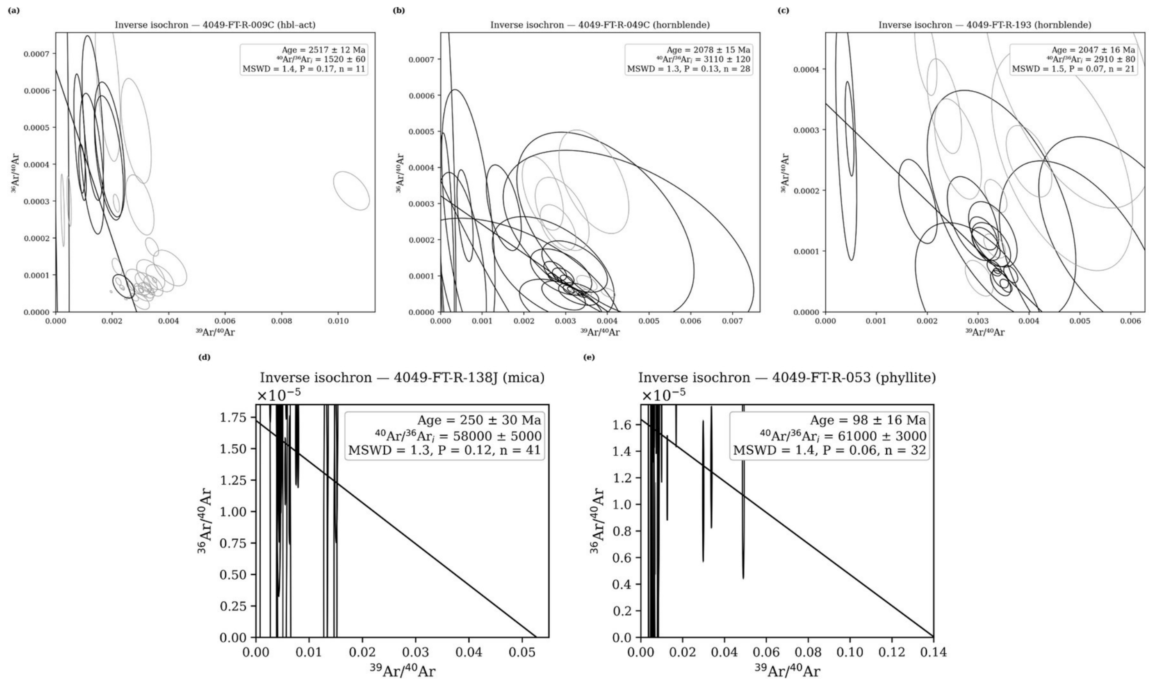

Fig. S2. Inverse-isochron and disturbed-reservoir regressions. (a–c) Preferred inverse-isochron ages for the excess-argon amphiboles FT-009C, FT-049C and FT-193. The secondary 2199 ± 25 Ma and younger 2087 ± 31 Ma FT-009C arrays are shown in main-text Fig. 6c and tabulated with exact selections in Table S2; only the preferred FT-009C fit is repeated here. (d–e) Disturbed-reservoir regressions for FT-138J and FT-053, which constrain younger Mesozoic disturbance and are not preferred tectonic ages. Same conventions as Fig. 6.

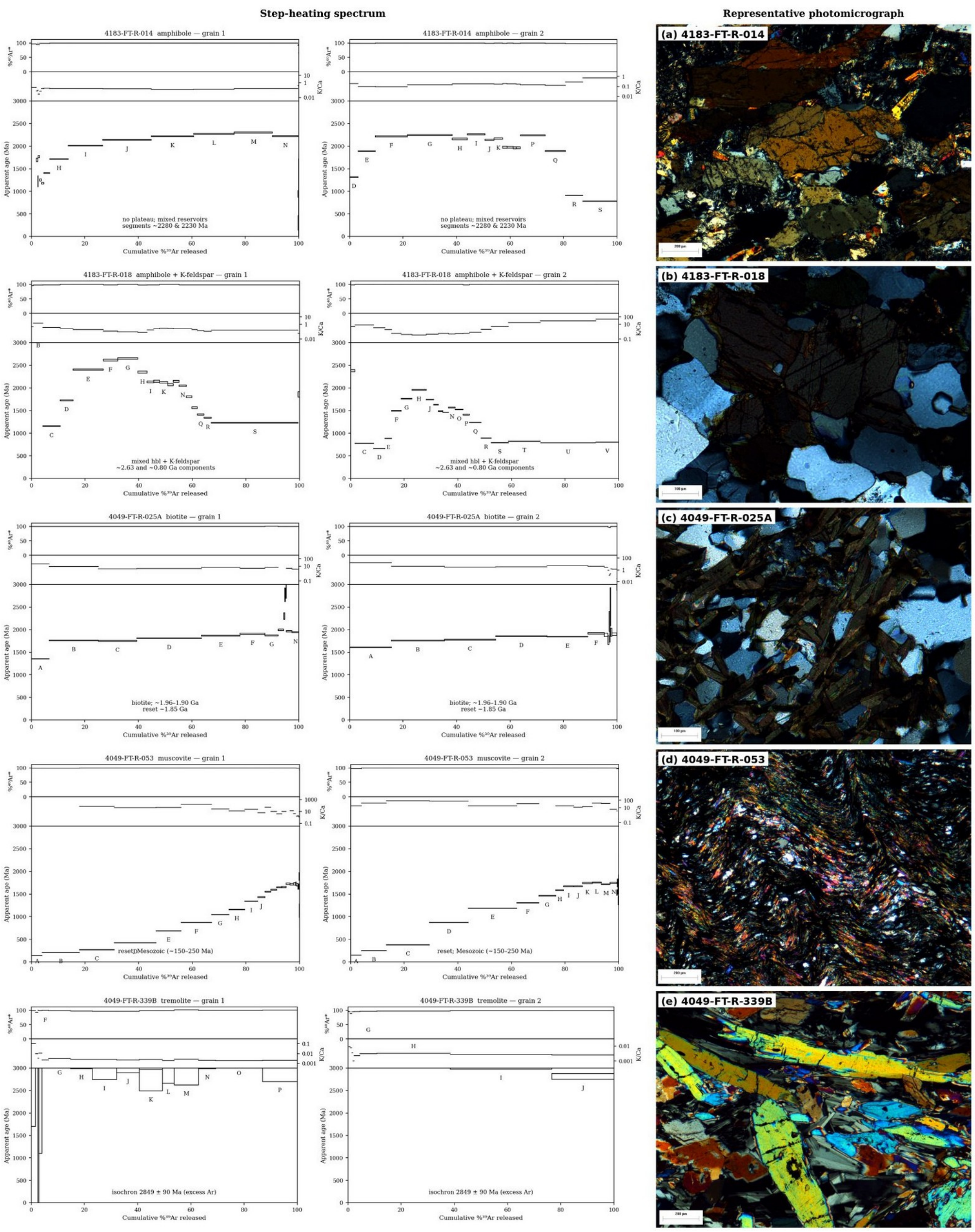

Fig. S3. Step-heating spectra and representative photomicrographs of the non-anchor samples (FT-025A, -053, -339B; FT-014, -018), which record additional thermal components of the archive discussed in Section 5.7.

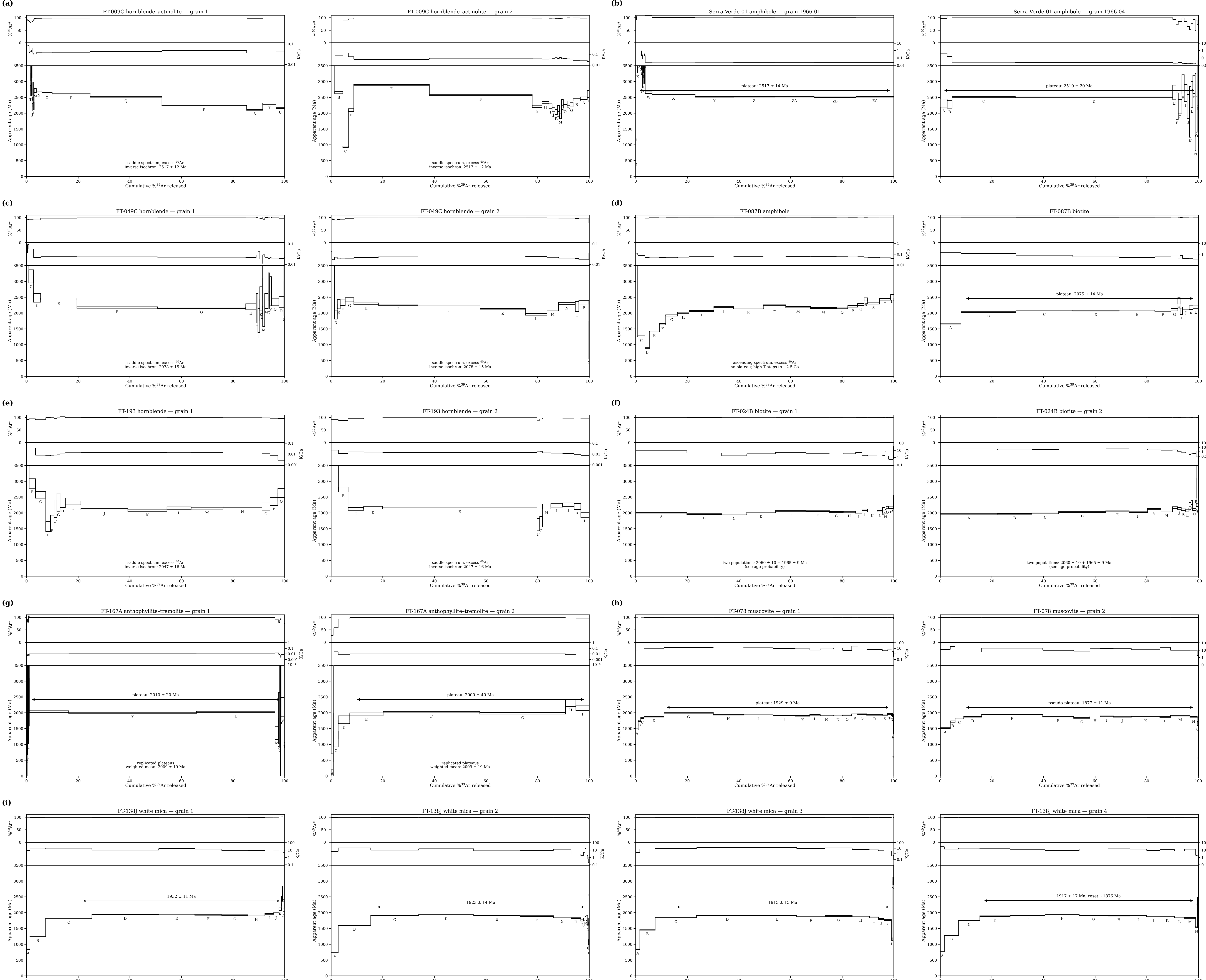
(a)
FT-009C hornblende–actinolite — grain 1
saddle spectrum, excess ^{40}Ar
inverse isochron: 2517 ± 12 Ma
FT-009C hornblende–actinolite — grain 2
saddle spectrum, excess ^{40}Ar
inverse isochron: 2517 ± 12 Ma
(b)
Serra Verde-01 amphibole — grain 1966-01
plateau: 2517 ± 14 Ma
Serra Verde-01 amphibole — grain 1966-04
plateau: 2510 ± 20 Ma
(c)
FT-049C hornblende — grain 1
saddle spectrum, excess ^{40}Ar
inverse isochron: 2078 ± 15 Ma
FT-049C hornblende — grain 2
saddle spectrum, excess ^{40}Ar
inverse isochron: 2078 ± 15 Ma
(d)
FT-087B amphibole
ascending spectrum, excess ^{40}Ar
no plateau; high-T steps to ~2.5 Ga
FT-087B biotite
plateau: 2075 ± 14 Ma
(e)
FT-193 hornblende — grain 1
saddle spectrum, excess ^{40}Ar
inverse isochron: 2047 ± 16 Ma
FT-193 hornblende — grain 2
saddle spectrum, excess ^{40}Ar
inverse isochron: 2047 ± 16 Ma
(f)
FT-024B biotite — grain 1
two populations: 2060 ± 10 + 1965 ± 9 Ma
(see age-probability)
FT-024B biotite — grain 2
two populations: 2060 ± 10 + 1965 ± 9 Ma
(see age-probability)
(g)
FT-167A anthophyllite–tremolite — grain 1
plateau: 2010 ± 20 Ma
replicated plateaus
weighted mean: 2009 ± 19 Ma
FT-167A anthophyllite–tremolite — grain 2
plateau: 2000 ± 40 Ma
replicated plateaus
weighted mean: 2009 ± 19 Ma
(h)
FT-078 muscovite — grain 1
plateau: 1929 ± 9 Ma
FT-078 muscovite — grain 2
pseudo-plateau: 1877 ± 11 Ma
(i)
FT-138J white mica — grain 1
1932 ± 11 Ma
FT-138J white mica — grain 2
1923 ± 14 Ma
FT-138J white mica — grain 3
1915 ± 15 Ma
FT-138J white mica — grain 4
1917 ± 17 Ma; reset ~1876 Ma
% ^{40}Ar*
K/Ca
Apparent age (Ma)
Cumulative %^{39}Ar released

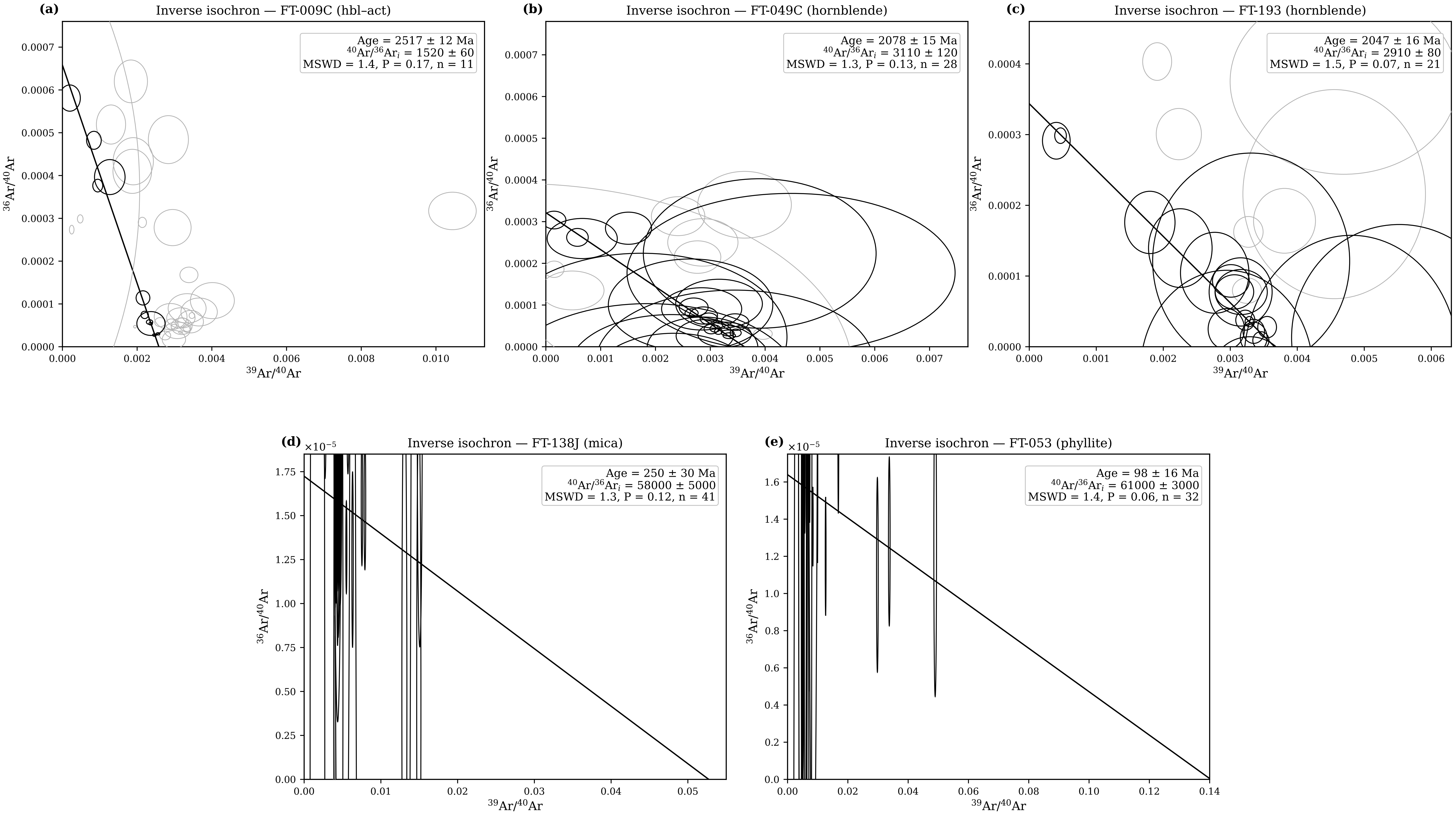
(a)
Inverse isochron — FT-009C (hbl–act)
Age = 2517 ± 12 Ma
$^{40}Ar/^{36}Ar_i$ = 1520 ± 60
MSWD = 1.4, P = 0.17, n = 11
$^{36}Ar/^{40}Ar$
$^{39}Ar/^{40}Ar$
(b)
Inverse isochron — FT-049C (hornblende)
Age = 2078 ± 15 Ma
$^{40}Ar/^{36}Ar_i$ = 3110 ± 120
MSWD = 1.3, P = 0.13, n = 28
$^{36}Ar/^{40}Ar$
$^{39}Ar/^{40}Ar$
(c)
Inverse isochron — FT-193 (hornblende)
Age = 2047 ± 16 Ma
$^{40}Ar/^{36}Ar_i$ = 2910 ± 80
MSWD = 1.5, P = 0.07, n = 21
$^{36}Ar/^{40}Ar$
$^{39}Ar/^{40}Ar$
(d)
Inverse isochron — FT-138J (mica)
$\times 10^{-5}$
Age = 250 ± 30 Ma
$^{40}Ar/^{36}Ar_i$ = 58000 ± 5000
MSWD = 1.3, P = 0.12, n = 41
$^{36}Ar/^{40}Ar$
$^{39}Ar/^{40}Ar$
(e)
Inverse isochron — FT-053 (phyllite)
$\times 10^{-5}$
Age = 98 ± 16 Ma
$^{40}Ar/^{36}Ar_i$ = 61000 ± 3000
MSWD = 1.4, P = 0.06, n = 32
$^{36}Ar/^{40}Ar$
$^{39}Ar/^{40}Ar$

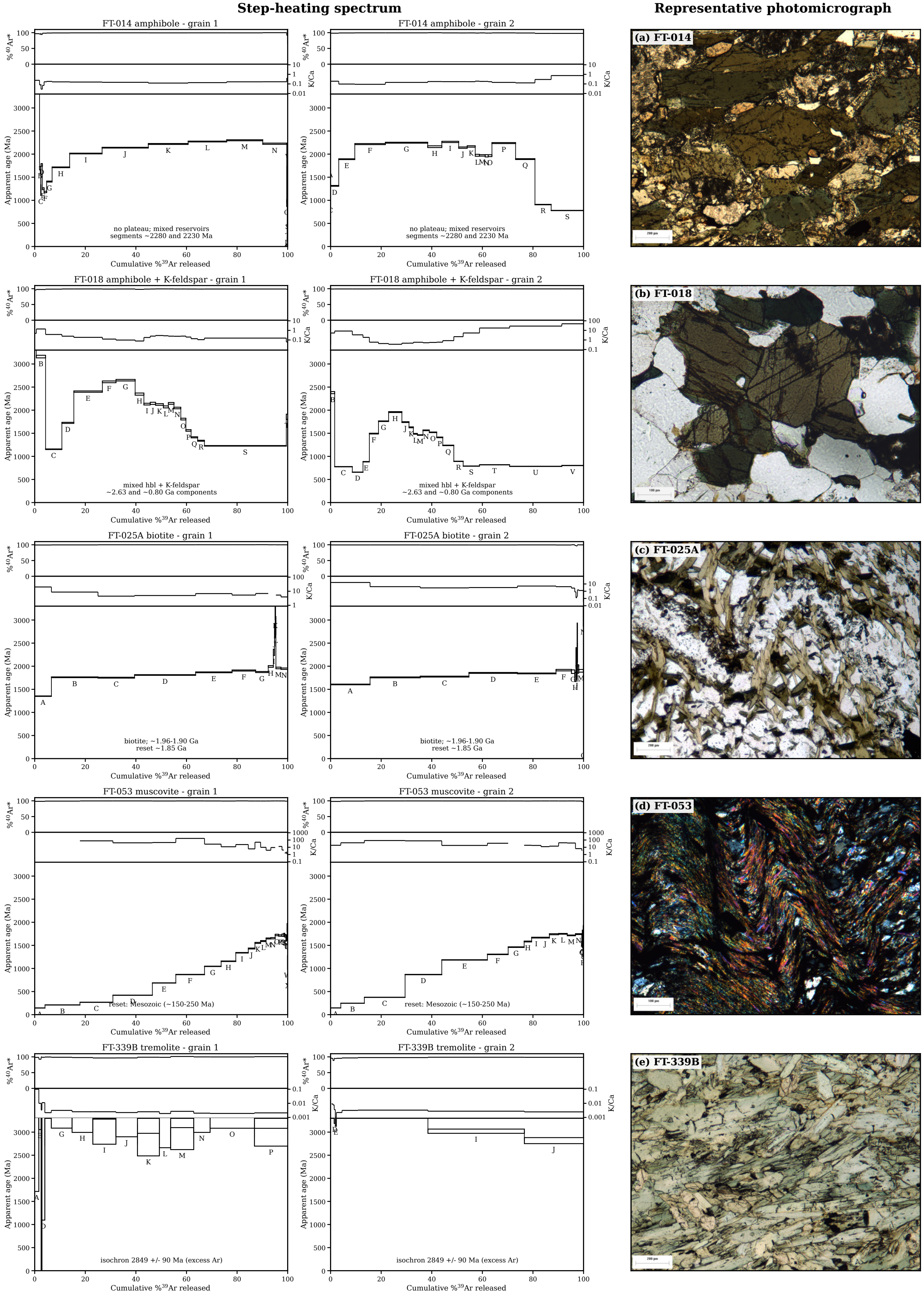
Step-heating spectrum
Representative photomicrograph
FT-014 amphibole - grain 1
FT-014 amphibole - grain 2
no plateau; mixed reservoirs
segments ~2280 and 2230 Ma
(a) FT-014
FT-018 amphibole + K-feldspar - grain 1
FT-018 amphibole + K-feldspar - grain 2
mixed hbl + K-feldspar
~2.63 and ~0.80 Ga components
(b) FT-018
FT-025A biotite - grain 1
FT-025A biotite - grain 2
biotite; ~1.96-1.90 Ga
reset ~1.85 Ga
(c) FT-025A
FT-053 muscovite - grain 1
FT-053 muscovite - grain 2
reset: Mesozoic (~150-250 Ma)
(d) FT-053
FT-339B tremolite - grain 1
FT-339B tremolite - grain 2
isochron 2849 +/- 90 Ma (excess Ar)
(e) FT-339B
%40Ar*
K/Ca
Apparent age (Ma)
Cumulative %39Ar released